An advanced change detection method for time-series soil moisture retrieval from Sentinel-1

Liujun Zhu [a,b,c,*], Rui Si [a,d], Xiaoji Shen [a,b], Jeffrey P. Walker [b]

[a] *Yangtze Institute for Conservation and Development, Hohai University, Nanjing, China*
[b] *Department of Civil Engineering, Monash University, Clayton, Vic. 3800, Australia*
[c] *State Key Laboratory of Hydrology-Water Resources and Hydraulic Engineering, Nanjing Hydraulic Research Institute, Nanjing 210029, China*
[d] *College of Hydrology and Water Resources, Hohai University, Nanjing, 210098, China*

ARTICLE INFO

ABSTRACT

The feasibility of soil moisture retrieval from C-band Sentinel-1 data has been widely acknowledged, with pre-operational 1-km products currently available at regional and/or continental scale using the long-term (LTCD) or short-term change detection (STCD) methods. Both algorithms share the same assumptions of time-invariant roughness and vegetation, which can be questionable even for a short period of 4 Sentinel-1 acquisitions (18–36 days). An advanced change detection (ACD) method is proposed in this study for an improved soil moisture retrieval from Sentinel-1 data, including two main modifications with respect to the existing STCD methods: i) approximating the effect of temporal varying vegetation on the Sentinel-1 backscatter as a variation in the two-way attenuation, and ii) a temporal soil moisture constraint based on the coarse Soil Moisture Active Passive (SMAP) soil moisture product to partly remove the uncertainty caused by vegetation and/or roughness changes. The evaluation, based on time-series observations from 34 OzNet stations and ground samples collected during the Fifth Soil Moisture Active and Passive Experiment (SMAPEx-5) showed that the ACD improved the correlation coefficient (R), root mean square error (RMSE) and un biased RMSE (ubRMSE), achieving 0.66, 0.071 m^3/m^3 and 0.071 m^3/m^3 at the point scale, 0.77, 0.063 m^3/m^3 and 0.051 m^3/m^3 at 1-km scale, 0.80, 0.055 m^3/m^3 and 0.050 m^3/m^3 at 3-km scale. The contribution of the two modifications was further investigated using 559 stations from 22 networks across the world, showing that: i) the two modifications can increase R by 0.08–0.13 and reduce the retrieval RMSE by 0.009–0.013 m^3/m^3 (10% - 15% relative), and ii) the retrieval over densely vegetated areas or areas with large temporal vegetation variation can benefit more from the proposed modifications. The ACD achieved stable performance for various Sentinel-1 orbits/passes and maintained a stable performance for retrieval windows up to 30 Sentinel-1 acquisitions, providing a promising alternative for achieving consistent soil moisture retrievals from Sentinel-1.

1. Introduction

Soil moisture products with high spatial ($<$ 1 km) and temporal (2–3 days) resolution are required in various sectors (Peng et al., 2020). Currently, globally available remote sensing soil moisture products include those produced from space-borne scatterometers (Bartalis et al., 2007), radiometers (Entekhabi et al., 2010; Kerr et al., 2010) and/or their combinations (Dorigo et al., 2017; Yao et al., 2021), with a low spatial resolution of 10s km. Considerable effort on downscaling algorithms has led to spatially enhanced soil moisture products, but they do not yet meet expectations (Peng et al., 2017; Sabaghy et al., 2018), particularly at kilometer resolution.

Recent advances in space-borne Synthetic Aperture Radars (SAR), especially an enhanced revisit and emerging open data policy, enables a promising alternative. Pre-operational 1-km soil moisture products are now available at regional to continental scale using SAR data from the Sentinel-1 constellation (Balenzano et al., 2021; Bauer-Marschallinger et al., 2018). These SAR-based products involve time-series data and share an assumption of time-invariant roughness and vegetation, which can be roughly classified into three categories.

The first category extends the snapshot methods of inversing scattering models (Kornelsen and Coulibaly, 2013) to multi-temporal ones (Fan et al., 2021; Kim et al., 2012; Pierdicca et al., 2010; Zhu et al., 2019b). Since the major unknowns representing the temporal variation
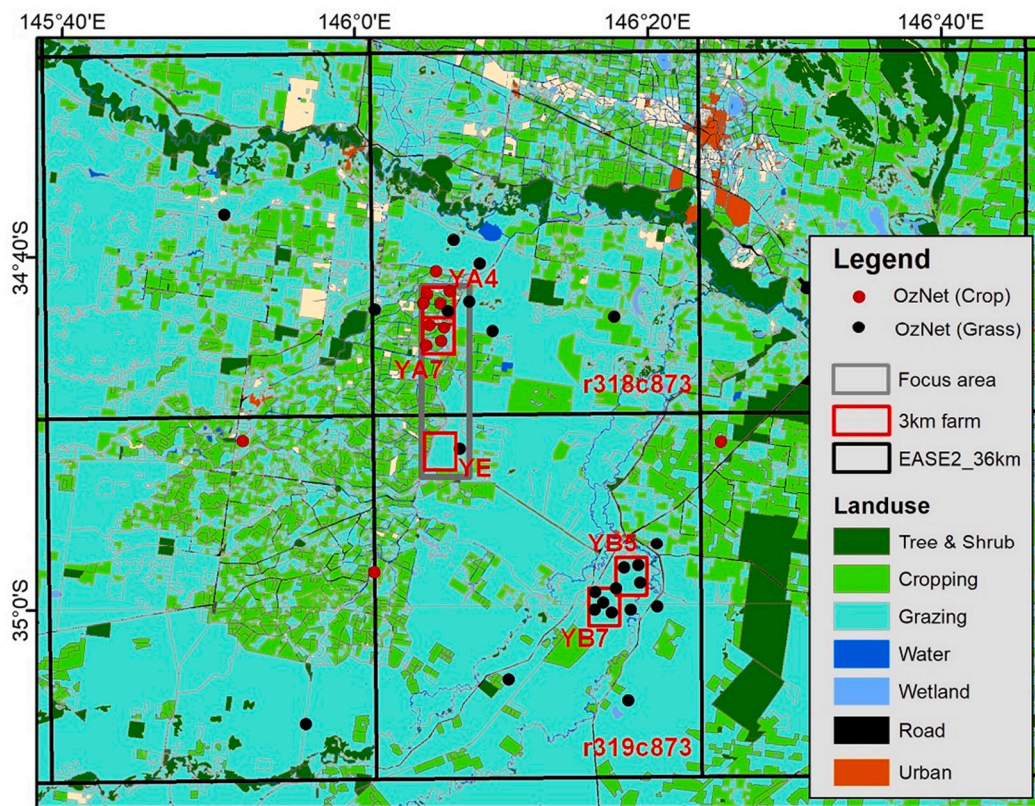
Fig. 1. The Yanco area and OzNet soil moisture stations, as well as the four focus farms with the most OzNet stations, the Equal-Area Scalable Earth (EASE-2) 36-km grids labeled by its row and column number (r318c873 and r319c873), the focus area of SMAPEx-5 experiment.

of roughness and vegetation were removed, the ill-posed inversion encountered in snapshot methods were converted into well-constrained inversions (Zhu et al., 2019a). To further constrain uncertainty of the data and scattering models, an ensemble retrieval framework was recently proposed where multiple soil moisture retrievals with moderate performance were first obtained using different channels and/or time instances, with the retrieved ensemble of results being the final output (Zhu et al., 2020b). Despite the satisfactory accuracy of these methods, reliable scattering models are still not readily available for large scale applications over a variety of landcover types at fine resolution.

The change detection algorithm initially proposed by Wagner et al. (1999b) determines the soil wetness in % by linearly scaling the observed backscatter between that at the driest and wettest conditions, captured from a long archive of backscatter collected by the same radar and configuration (frequency, polarization, incidence and azimuth angle). This algorithm and its variants (Tomer et al., 2015; Wagner et al., 1999a; Wagner et al., 1999b; Zribi et al., 2020) are thus also known as long-term change detection (LTCD) methods. In contrast, the alpha approximation method calculates absolute soil moisture by relating the ratio of two consecutive backscatter observations to the variation of soil moisture (Balenzano et al., 2011). To ensure time-invariant roughness and vegetation, the two consecutive observations are commonly collected within a short time interval (e.g., two weeks), with it thus known as the short-term change detection (STCD) method. The initial single polarization STCD has been extended to include multi-polarized data and various techniques to bound the radar-derived soil moisture (Al-Khaldi et al., 2019; Balenzano et al., 2021; Balenzano et al., 2013; He et al., 2017; Ouellette et al., 2017).

The validity of the time-invariant roughness and vegetation assumption is the key to the success of these time series methods. Although soil roughness in agricultural fields changes gradually after soil tillage due to various erosion processes (Jackson et al., 1997), many

field experiments have confirmed that such changes are negligible from a few weeks to an entire crop season (Callens et al., 2006; Njoku et al., 2002; Ye et al., 2020). Accordingly, time-invariant roughness can be safely assumed in STCD methods and scattering model based time series methods, but is questionable for LTCD methods, especially at high spatial resolutions of <1 km.

As for vegetation, its water content (VWC) and structure change much more quickly than soil roughness. For example, the growth of wheat can be roughly divided into six stages, each spanning 10–40 days (Acevedo et al., 2002). While many SAR constellations can collect tens of acquisitions within a growth stage, e.g., the Cosmo SkyMed, they are of little value for operational soil moisture mapping due to the data acquisition strategy. Sentinel-1 is currently the most advanced SAR mission to support a surface soil moisture product with high spatial resolution, having a revisit of 6 or 12 days depending on the availability of acquisitions from one or two satellites (Torres et al., 2012). The capability of Sentinel-1 for soil moisture retrieval has been widely acknowledged using change detection methods (e.g., Gao et al., 2017; Palmisano et al., 2020), machine learning (e.g., Cui et al., 2021; Paloscia et al., 2013) and/or scattering model based methods (e.g., Bousbih et al., 2018; Cui et al., 2021) at a resolution up to 30 m. Existing applications of STCD methods are mostly confined to 4 Sentinel-1 acquisitions (Balenzano et al., 2021; Palmisano et al., 2020), resulting in a retrieval time window of 18 or 36 days. The potential vegetation variation within 36 days would therefore have a substantial effect on the STCD methods.

To overcome the above challenges, the STCD was reformulated in this study to partly include the effect of temporal vegetation evolution, for improved operational soil moisture retrieval using C-band Sentinel-1 data. For the vegetated areas dominated by soil scattering, the effect of temporal vegetation variation on time series Sentinel-1 VV was approximated as the variation of two-way attenuation, which was then removed using a second order ratio of three consecutive backscatter

Table 1

Summary of the 22 networks used for the extended evaluation.

Network (Reference or Website)	# Station	# mv measurements	LULC*	# time series Asc./ Des.	Incidence angle**
AMMA-CATCH (Galle et al., 2018)	7	635	3, 7, 8	10/0	41.0 ± 5.5
ARM (Cook, 2016)	15	2490	2, 3	19/0	38.3 ± 3.6
FLUXNET-AMERIFLUX (http://ameriflux.lbl.gov/)	5	1119	2, 3, 8	8/5	37.3 ± 4.2
FMI (Ikonen et al., 2018)	16	6731	2, 6	48/48	37.2 ± 4.4
FR_Aqui (Al-Yaari et al., 2018)	4	2369	2, 6, 8	4/8	36.5 ± 4.3
HOAL (Blöschl et al., 2016)	31	6720	3	31/31	38.7 ± 0.3
HOBE (Jensen and Refsgaard, 2018)	27	10,543	3, 6, 8	54/59	36.1 ± 4.6
MAQU (Su et al., 2011)	5	254	2	5/2	36.9 ± 1.1
NAQU (Su et al., 2011)	7	1036	2	14/7	37.6 ± 4.9
NGARI (Su et al., 2011)	14	1398	2, 5	13/15	36.5 ± 1.9
OzNet (Smith et al., 2012)	34	1039	2, 3	0/34	37.9 ± 1.7
PBO_H2O (Larson et al., 2008)	30	1947	1, 2, 3, 8	36/17	38.2 ± 4.0
REMEDHUS (González-Zamora et al., 2019)	20	10,574	1, 2, 3, 8	31/20	38.5 ± 4.2
RISMA (Ojo et al., 2015)	22	2194	2, 3	39/0	36.9 ± 4.4
RSMN (http://assimo.meteoromania.ro)	19	9999	3, 4, 7, 8	33/33	38.9 ± 4.6
Ru_CFR	1	48	7	0/1	34.7 ± 0.0
SCAN (Schaefer et al., 2007)	168	21,832	1, 2, 3, 4, 5, 6, 7, 8	216/96	38.4 ± 4.2
SMOSMANIA (Calvet et al., 2016)	21	12,749	1, 3, 8	33/32	38.0 ± 4.5
TAHMO (https://tahmo.org/)	4	159	1, 4, 6	4/0	39.1 ± 3.2
TERENO (Zacharias et al., 2011)	4	2509	3, 8	6/8	38.1 ± 4.6
USCRN (Bell et al., 2013)	99	14,675	1, 2, 3, 5, 6, 7, 8	135/68	38.3 ± 4.4
iRON (Osenga et al., 2019)	6	817	2, 6, 8	10/8	39.2 ± 4.7
Total	559	111,837		749/492	

* : 1–8 refers to shrubs, grass, crop, bare, urban, evergreen forest, deciduous forest and mixed forest, respectively.

** : Average value± Standard deviation.

Table 2

Summary of the change detection algorithms compared in this study.

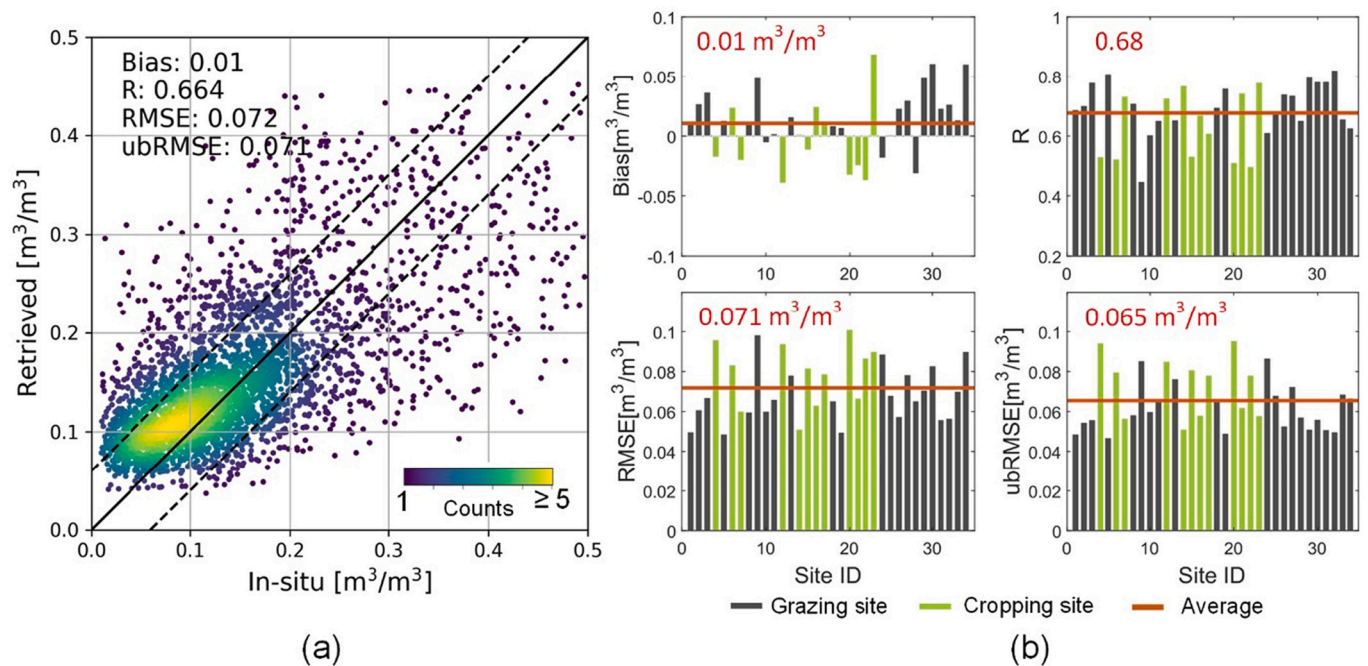| Algorithm	Linear equations	Constraints
Sort term change detection (STCD)	Eq. 5	$0.03 \leq mv \leq 0.5$
STCD with soil moisture bounds (STCD_B)	Eq. 5	$mv_{min}^{SMAP} \leq mv \leq mv_{max}^{SMAP}$
STCD_B with time-varying vegetation (STCD_V)	Eq. 9	$mv_{min}^{SMAP} \leq mv \leq mv_{max}^{SMAP}$
STCD_B with temporal constraints (STCD_T)	Eq. 5	Eq. 14 and 15
Advanced change detection (ACD)	Eq. 9	Eq. 14 and 15

Fig. 2. (a) Retrieved soil moisture versus OzNet observations, with the solid line and dashed lines indicating 1:1 and the ± 0.06 m³/m³ margins respectively. (b) Retrieval statistic of each station, with the red line and value being the average of all stations. (For interpretation of the references to colour in this figure legend, the reader is referred to the web version of this article.)

acquisitions and the corresponding time series of normalized difference vegetation index (NDVI). Moreover, the soil moisture active passive (SMAP) L2 passive only soil moisture product was used to provide a temporal constraint of the inversion process, as an extension of the constraints proposed by Ouellette et al. (2017) and Zhu et al. (2019b). The STCD method with the two modifications was named the advanced change detection (ACD) method. It is expected to provide more reliable soil moisture retrievals than the existing STCDs while maintaining the capability of global application in an operational manner.

The proposed ACD was first evaluated using in-situ soil moisture data collected in the Yanco agricultural area, including time series observations from 34 OzNet stations and ground samples collected during the Fifth Soil Moisture Active and Passive Experiment (SMAPEx-5). Moreover, the ACD, the two STCD variants using each of the two modifications separately, and the two existing STCD variants (Balenzano et al., 2013; Ouellette et al., 2017) were compared to each other and evaluated on 559 stations from 22 soil moisture monitoring networks, providing a deep investigation of the proposed modifications, including the effect of vegetation, incidence angle and orbit direction (ascending and descending).

2. Methodology

2.1. Short-term change detection (STCD)

The short-term change detection method is also known as the alpha approximation approach for soil moisture retrieval (Balenzano et al., 2011), starting from a first-order approximation of the radiative transfer (RT) theory. The total backscattering coefficient at VV polarization can be expressed as the sum of three terms in linear units as:

$$\sigma_{VV}^{total} = \sigma_{VV}^s \gamma^2 + \sigma_{VV}^v + \sigma_{VV}^{sv} \tag{1}$$

where the first term of the right side is the soil surface scattering attenuated by the vegetation canopy, with the γ^2 being the two-way vegetation attenuation. The second and third terms are the volume scattering from the vegetation canopy and the multiple scattering between the vegetation and soil surface, respectively. A preprocessing step of removing areas dominated by volume scattering (Satalino et al., 2014) can therefore be applied to simplify Eq. 1 to:

$$\sigma_{VV}^{total} \approx \sigma_{VV}^s \gamma^2 = |\alpha_{VV}(\varepsilon, \theta)|^2 \cdot \Omega \cdot \gamma^2 \tag{2}$$

where $\alpha_{VV}(\varepsilon, \theta)$ is the reflection coefficient, representing the effect of soil permittivity (ε) and incidence angle (θ). The term Ω represents the influence of soil surface roughness. Since roughness and vegetation can be assumed time-invariant for a short period, the backscatter ratio of two subsequent VV acquisitions $S_{i+1,i}$ at DoY i and DoY $i + 1$ is:

$$S_{i+1,i} = \frac{\sigma_{VV,i+1}^{total}}{\sigma_{VV,i}^{total}} \approx \frac{\sigma_{VV,i+1}^s \gamma^2}{\sigma_{VV,i}^s \gamma^2} \approx \frac{|\alpha_{VV,i+1}(\varepsilon, \theta)|^2}{|\alpha_{VV,i}(\varepsilon, \theta)|^2} \tag{3}$$

with

$$|\alpha_{VV}(\varepsilon, \theta)| = \left| \frac{(\varepsilon - 1)(sin^2\theta - \varepsilon(1 + sin^2\theta))}{\left(\varepsilon cos\theta + \sqrt{\varepsilon - sin^2\theta}\right)^2} \right| \tag{4}$$

For simplicity, α is used to represent $\alpha_{VV}(\varepsilon, \theta)$ hereafter. Given a time series of N Sentinel-1 VV acquisitions, the time series of α can be solved using:

$$\begin{bmatrix} -\sqrt{S_{2,1}} & 1 & 0 & \cdots & 0 & 0 \\ 0 & -\sqrt{S_{3,2}} & 1 & \cdots & 0 & 0 \\ \cdots & \cdots & \cdots & \cdots & \cdots & \cdots \\ 0 & 0 & 0 & 0 & -\sqrt{S_{N,N-1}} & 1 \end{bmatrix} \begin{bmatrix} \alpha_1 \\ \alpha_2 \\ \cdots \\ \alpha_{N-1} \\ \alpha_N \end{bmatrix} = \overrightarrow{0} \tag{5}$$

where $\overrightarrow{0}$ is the null vector with a length of N -1. Obviously, Eq. 5 is underdetermined, with N -1 equations and N unknowns. To constrain this underdetermined stochastic system, be constrained by applying a set of linear can be applied:

$$\alpha_{min} \leq \alpha_i \leq \alpha_{max}, \quad i = 1 \ldots N \tag{6}$$

where α_{min} and α_{max} are calculated from the soil texture properties. In the Soil MOisture retrieval from multi-temporal SAR data (SMOSAR) proposed by Balenzano et al. (2012), N is set as a fixed value of 4 considering the tradeoff between the validity of the time invariant assumptions and the fact that a longer time series introduces more observations. However, substantial vegetation changes can occur within the 18 days or 36 days time span of 4 Sentinel-1 acquisitions.

2.2. Advanced change detection (ACD)

Similar to the STCD, the proposed advanced change detection method applies to bare or vegetated soils dominated by attenuated surface scattering. Roughness is also assumed to be time invariant as it is relatively stable for a crop season (a few months). However, the variation of two-way vegetation attenuation is considered to reflect the effect of vegetation variation in time. The two-way vegetation attenuation (Attema and Ulaby, 1978) can be expressed as:

$$\gamma^2 = exp(-2AVsec\theta) \tag{7}$$

where A is an empirical parameter depending on the radar configuration and vegetation type, and V is a bulk vegetation descriptor, which can be leaf area index (LAI), vegetation water content (VWC) or NDVI (Joseph et al., 2010; Qiu et al., 2019). Considering the attenuation, Eq. 3 becomes:

$$S_{i+1,i} \approx \frac{|\alpha_{VV,i+1}|^2 exp(-2AV_{i+1}sec\theta)}{|\alpha_{VV,i}|^2 exp(-2AV_i sec\theta)} \tag{8}$$

Since V can be obtained from other remote sensing data or products and the parameter A is independent of time, it is possible to write a linear underdetermined system of N - 2 equations with N unknowns ln

$$\begin{bmatrix} -2 & 2\omega_{3,1} + 2 & -2\omega_{3,1} & 0 & \cdots & 0 & 0 & 0 \\ 0 & -2 & 2\omega_{4,2} + 2 & -2\omega_{4,2} & \cdots & 0 & 0 & 0 \\ \cdots & \cdots & \cdots & \cdots & \cdots & \cdots & \cdots & \cdots \\ 0 & 0 & 0 & 0 & \cdots & -2 & 2\omega_{N,N-2} + 2 & -2\omega_{N,N-2} \end{bmatrix} \begin{bmatrix} ln(\alpha_1) \\ ln(\alpha_2) \\ \cdots \\ ln(\alpha_N) \end{bmatrix}$$

$$= \begin{bmatrix} ln(S_{2,1}) - \omega_{3,1} ln(S_{3,2}) \\ ln(S_{3,2}) - \omega_{4,2} ln(S_{4,3}) \\ \cdots \\ ln(S_{N-1,N-2}) - \omega_{N,N-2} ln(S_{N,N-1}) \end{bmatrix} \tag{9}$$
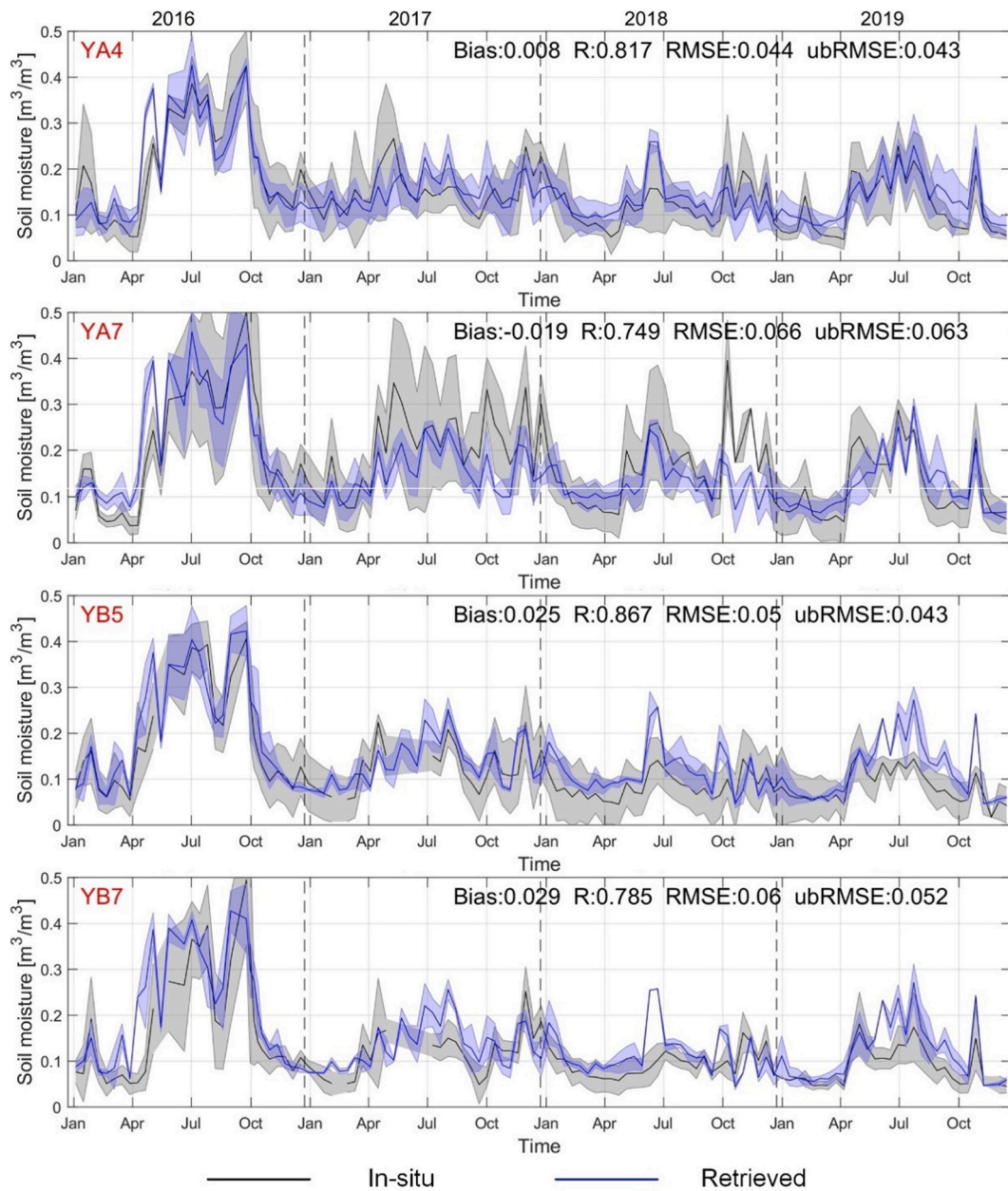
Fig. 3. Averaged OzNet observations within each 3-km focus farm (blue) and the corresponding retrieved soil moisture (black). Envelopes represent the standard deviation related to the average value. (For interpretation of the references to colour in this figure legend, the reader is referred to the web version of this article.)

(α_N) (see appendix for the complete derivation and the case $V_{i+2} = V_{i+1}$):

with

$$\omega_{i+2,i} = (V_{i+1} - V_i)/(V_{i+2} - V_{i+1}), (V_{i+2} \neq V_{i+1}) \tag{10}$$

Obviously, Eq. 9 requires at least 3 consecutive SAR acquisitions and Eq. 5 can be treated as a special case of Eq. 9 when $\omega_{i+2,i}$ equals to 0:

$$\begin{bmatrix} -2 & 2 & 0 & \dots & 0 & 0 \\ 0 & -2 & 2 & \dots & 0 & 0 \\ \dots & \dots & \dots & \dots & \dots & \dots \\ 0 & 0 & 0 & 0 & -2 & 2 \end{bmatrix} \begin{bmatrix} ln(\alpha_1) \\ ln(\alpha_2) \\ \dots \\ ln(\alpha_N) \end{bmatrix} = \begin{bmatrix} ln(S_{2,1}) \\ ln(S_{3,2}) \\ \dots \\ ln(S_{N,N-1}) \end{bmatrix} \tag{11}$$

This suggests that Eq. 9 is also valid for bare soil, time invariant vegetation and retrieval periods with bare-vegetation transitions, except the case that only one vegetated time instance is available because at least two vegetated time instances are required to remove the parameter

A. While various bulk vegetation descriptors (V) can be directly used in Eq. 9, a preprocessing step of identifying the crop season is required for vegetation indices (e.g., NDVI).

It is widely acknowledged that an accurate initial estimate of the upper and lower bound soil moisture values is crucial for successful soil moisture retrieval (Al-Khaldi et al., 2019; Balenzano et al., 2021; He et al., 2017; Ouellette et al., 2017). Use of the full range (0.03–0.5 m^3/m^3) in Eq. 6 tended to underestimate soil moisture, with most retrievals being near the minimal bound (Ouellette et al., 2017). Accordingly, in this study the minimum and maximum soil moisture derived from SMAP products were used to determine the α_{min} and α_{max} (Ouellette et al., 2017). Specifically, given a retrieval period with N SMAP observations the minimum and the maximum soil moisture were determined as:

$$mv_{min} = min(mv_1^{SMAP}, \dots, mv_N^{SMAP}, mv_{ave}), \tag{12}$$

$$mv_{max} = max(mv_1^{SMAP}, \dots, mv_N^{SMAP}, mv_{ave}), \tag{13}$$
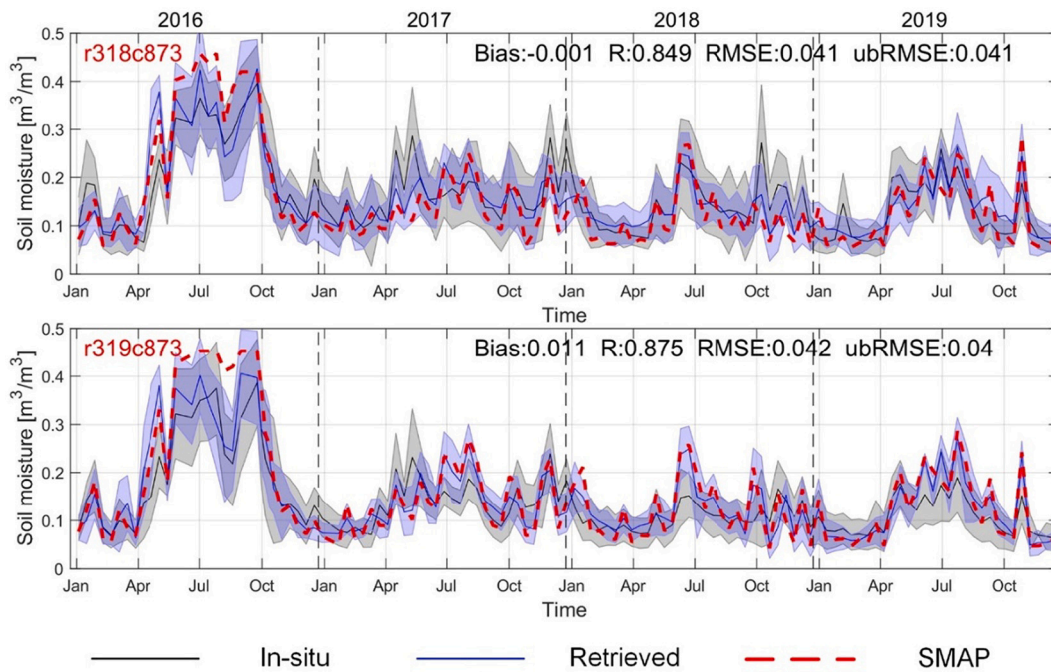
Fig. 4. Time series OzNet observations, retrieved soil moisture and SMAP data of two 36 km EASE grids (r319c873 and r318c873) from 2016 to 2019. Envelopes represent the standard deviation related to the average value.

where mv_{ave} is the average soil moisture of all historical SMAP records of the area of interest. The assumption behind this constraint is that the coarse soil moisture range of a retrieval period is similar to the range of high-resolution soil moisture within the coarse grid. For a long enough retrieval period (e.g., 3 years), the use of minimum and maximum soil moisture is similar to the LTCD method (Wagner et al., 1999b), which involved the driest and wettest scenarios. This was found to over-estimate the ranges for dry or wet seasons (Ouellette et al., 2017) and thus only the SMAP observations collected during the retrieval period were used. However, the coarse soil moisture of a short period in dry (wet) seasons can be a constantly low (high) value, substantially underestimating the range of the soil moisture at high resolution. Consequently, the mv_{ave} was included in the calculation of bounds, which is expected to provide a relatively large range for a dry or wet season and thus "anomalies" (e.g., high values after irrigation in a dry season) at a fine resolution can be captured.

The time series of α is also forced to follow the soil moisture trend of the SMAP products, being a variant of the dry down constraint proposed in Zhu et al. (2019b). Given two time-instances i and j with $mv_j^{SMAP} \geq mv_i^{SMAP}$, a set of linear constraints can be used to further constrain the retrieval, such that:

$$\alpha_{min} \leq \alpha_i \leq \alpha_j \leq \alpha_{max}, i, j \in (1, 2, \ldots, N) \tag{14}$$

The rationale is that soil moisture within a 36-km grid can share a similar monotonic dry down process after a rainfall event. However, farm-scale irrigation events and/or sub-grid scale rainfall can result in different soil moisture trends within a 36-km grid. The empirical rule proposed by Bazzi et al. (2020):

$$\sigma_{i+1} - \sigma_i \geq 1 \text{ dB and } mv_i^{SMAP} \geq mv_{i+1}^{SMAP} \tag{15}$$

was used to detect highly confident sub-grid scale soil moisture anomalies. For a pixel meeting Eq. 15, irrigation or rainfall may occur at this pixel, resulting in a different temporal evolution for this pixel and the 36-km grid cell. Thus the minimum-maximum constraint of Eq. 6 was used instead of the temporal constraint (Eq. 14).

In implementing the proposed ADC, NDVI was selected as the vegetation descriptor due to its simplicity and the limited difference

when using other vegetation indices in the water cloud model (El Hajj et al., 2016; Qiu et al., 2019). An empirical rule of NDVI >0.2 was used to identify vegetated soils (Montandon and Small, 2008), with the vegetated soil dominated by volume scattering being removed using a fixed empirical threshold of HV > -14 dB (Satalino et al., 2014). A time series of $\ln(\alpha_N)$ can then be achieved by solving Eq. 9 using a least-squares optimization with the constraint of Eq. 14. Time series soil moisture was then calculated by inverting the Dobson et al. (1985) empirical model.

Following the multi-temporal retrieval scheme of Balenzano et al. (2013), given a time series of $M >> N$ acquisitions, a temporal moving window with a temporal step of 1 was used to extract $M - N + 1$ subsets of N acquisitions, and the soil moisture retrieved for each subset. The results of each subset were then averaged to yield the retrieved soil moisture. A default N of 4 was selected to be consistent with the existing STCDs (Al-Khaldi et al., 2019; Balenzano et al., 2021; Balenzano et al., 2013; He et al., 2017; Ouellette et al., 2017)., with the effect of larger N analyzed in Section 5.3.

3. Data and preprocessing

3.1. Soil moisture data and preprocessing

The soil moisture collected in the Yanco agricultural area, Australia were used in this study (Fig. 1). The Yanco area is a semi-arid cropping and grazing area, with the landcover type of grazing area being mainly grassland. The land cover type of cropping area has complex transitions, mainly including wheat in winter, corn and soybean in summer, and the possibility of fallow (bare soil with/without short grass) in any season. An extensive soil moisture monitoring network (OzNet) was established in this area since 2001, specifically for soil moisture remote sensing studies, with three main upgrades being in 2003, 2009 and 2018 (http://www.oznet.org.au). A total of 34 OzNet stations were used in this study (Fig. 1), covering a 4.5-year period from 1 August 2015 to 31 December 2019. Most of these stations were deployed in two 36-km Equal-Area Scalable Earth (EASE-2) grids (Fig. 1), i.e., r318c873 and r319c873 where r and c are row and column number of the 36-km EASE-
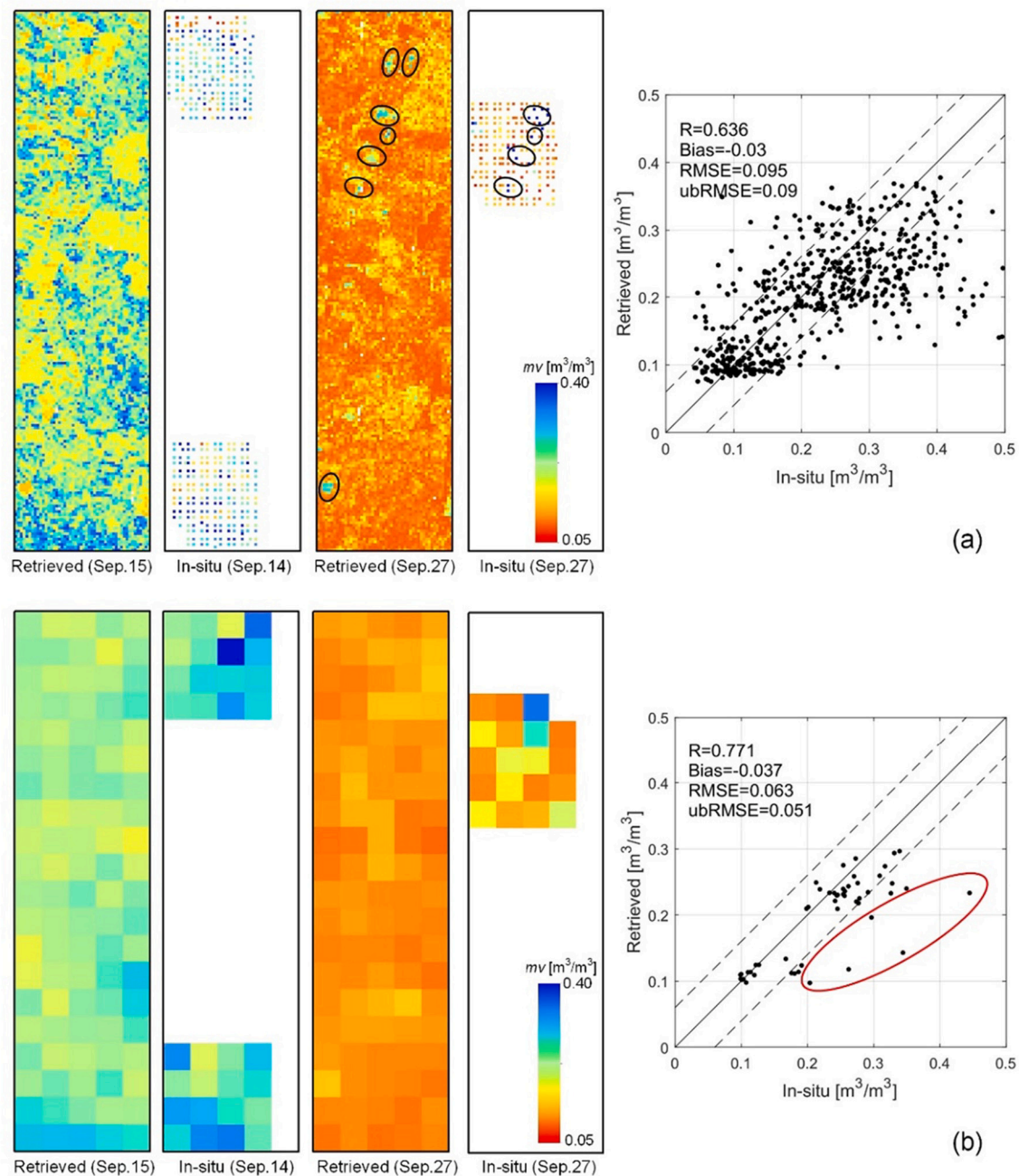
Fig. 5. SMAPEx5 intensive in-situ versus retrieved soil moisture at a resolution of 100 m (a) and 1000 m (b). The black circles in (a) are farms with irrigation on 27 September 2015. The solid lines on the scatter plots indicate the 1:1 line, while the dashed lines represent the ±0.06 m³/m³ margins. The points in the red circle in (b) are those with large underestimation caused by the scale mismatch between the in-situ and 1-km grid. (For interpretation of the references to colour in this figure legend, the reader is referred to the web version of this article.)

2 grid, respectively. A total of 14 soil moisture monitoring sites, located in the cropping area, were mainly clustered in two 3-km focus farms (YA4 and YA7). The size of crop fields ranged from 0.15 km² to 0.5 km² with the stations being deployed near the edges of individual fields. In contrast, the 20 stations on grassland are scattered in a relatively larger area, with the two YB focus farms containing 8 stations. The daily soil moisture at each station was first calculated by averaging the hourly measurements for the top 5 cm. Daily averaged soil moisture <0.03 m³/m³ or > 0.5 m³/m³ were then removed, considering the typical calibration error of 0.03 m³/m³ for stations (Smith et al., 2012).

Ground soil moisture measurements collected in the SMAPEx-5 were also used for evaluation, with a focus on spatial consistence. The SMAPEx-5 was conducted from 7 to 27 September 2015 for the calibration and validation of the SMAP concept (Ye et al., 2020). In the selected SMAPEx-5 focus area (5 × 20 km, the grey rectangle in Fig. 1), soil moisture was measured in the three 3-km focus farms YA4, YA7 and YE on a west-east oriented grid with a spacing of 250 m. Three replicate near surface (0–5 cm) soil moisture measurements were taken within 1 m distance at each sampling location using the Hydraprobe Data Acquisition System (HDAS, (Merlin et al., 2007), and averaged to account for spatial heterogeneity and sampling uncertainty. Two Sentinel-1 acquisitions were available for this period, being 15 and 27 September 2015 (UTC + 11) respectively, with nearly concurrent soil moisture measurements in YA4 and YE on the 14 and YA7 on 27 September. Similarly, measurements beyond the range of 0.03 to 0.5 m³/m³ were removed, resulting in a total of 608 soil moisture samples. Soil surface
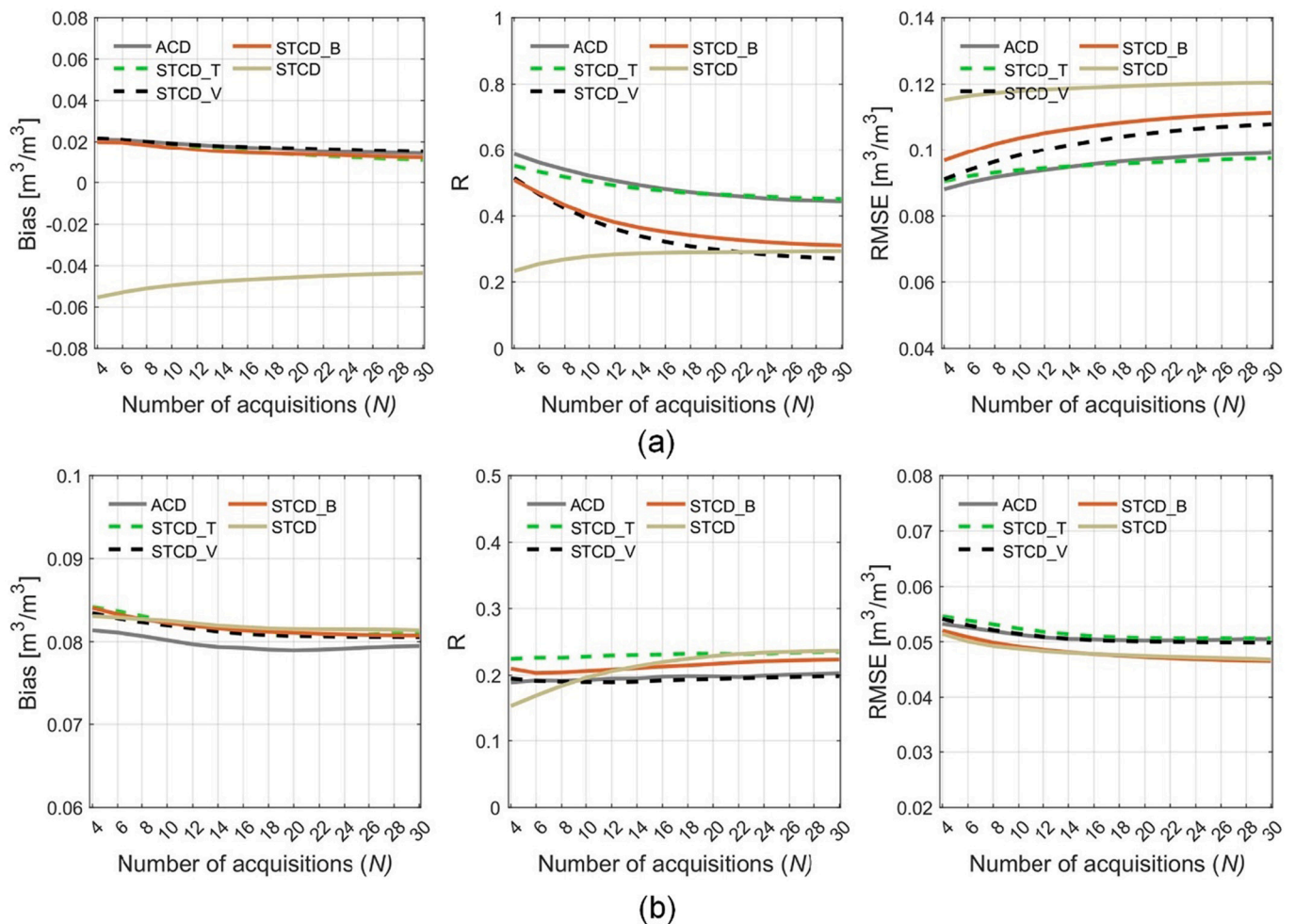
Fig. 6. Performance of the ACD, STCD_B, STCD, STCD_T, and STCD_V using different Sentinel-1 acquisitions. (a) and (b) are the average and standard deviation of statistics of 559 stations respectively.

roughness and vegetation samples were also collected in the focus farms and were found to change little over the duration of the campaign (Ye et al., 2020).

All the 0–5 cm soil moisture observations from the international soil moisture network (ISMN, (Dorigo et al., 2021) were considered in this study for a comprehensive evaluation. The soil moisture measurements collected during 2016–2019 were batch downloaded from the ISMN except those from Alaskan stations. Among the 1343 available stations, the 367 SNOTEL stations were filtered out because they were all installed in areas with complex terrain features, and accurate terrain correction and flattening was not undertaken for this study. Moreover, only the measurements with a quality flag of "G" (good) were used. Since the sensing depths varied across the stations, they were all assumed to represent the average soil moisture of the top 5 cm. As for the preprocessing of OzNet data, the daily soil moisture of each station was first calculated by averaging the hourly measurements of all sensors with a sensing depth of $\leq$ 5 cm. Any daily averaged soil moisture recordings out the range of 0.03–0.5 m^3/m^3 were then removed.

The land cover of each ISMN station was extracted from the Copernicus Global Land Cover Layers (CGLS-LC100 Collection 3, Buchhorn et al., 2020) using the Google Earth Engine (GEE); all the stations were observed to have consistent land cover types throughout the retrieval period of 2016–2019. The stations located in wetland and urban were then also removed, resulting in 559 stations from 22 networks (Table 1). For simplicity, the original 13 land cover types were categorized into 8 types, being shrubs, grass, crop, bare, urban, evergreen forest, deciduous

forest and mixed forest. Refer to https://github.com/rszlj/global_valida tion_of_soil_moisture_algorithm for the GEE based preparation of all the input data over the 559 stations.

3.2. Remote sensing data over the Yanco area

Three kinds of remote sensing data are required by the proposed ACD, being i) the Sentinel-1 backscatter data, ii) SMAP coarse soil moisture and iii) NDVI products. A total of 120 Sentinel-1A descending Interferometric Wide (IW) Ground Range (GRD) scenes acquired between 1 August 2015 and 31 December 2019 were used in this study, with a local incidence angle of around 38.5 deg. A standard GRD preprocessing workflow (Filipponi, 2019) was applied to each acquisition based on the Sentinel Application Platform (SNAP) and Geospatial Data Abstraction Library (GDAL), including i) apply orbit file; ii) thermal and GRD border noise removal; iii) radiometric calibration; iv) speckle filtering using a 5 × 5 median filter; v) terrain correction; and vi) splitting into granules (36 km × 36 km) based on the EASE-2.0 36-km grid. The preprocessed time series stacks of VV and VH backscatter coefficients were finally stored according to the 6 granules shown in Fig. 1 with a pixel size of 100 m. These data have ~100 looks with an expected radiometric accuracy of ~0.4 dB (Torres et al., 2012).

The SMAP L3 passive soil moisture product (Version 6, Neill et al., 2019) was used to provide the soil moisture constraints. The time series soil moisture of the 6 SMAP radiometer grid cells, i.e., r318c872, r318c873, r318c874, r319c872, r319c873, and r319c874 in Fig. 1, were
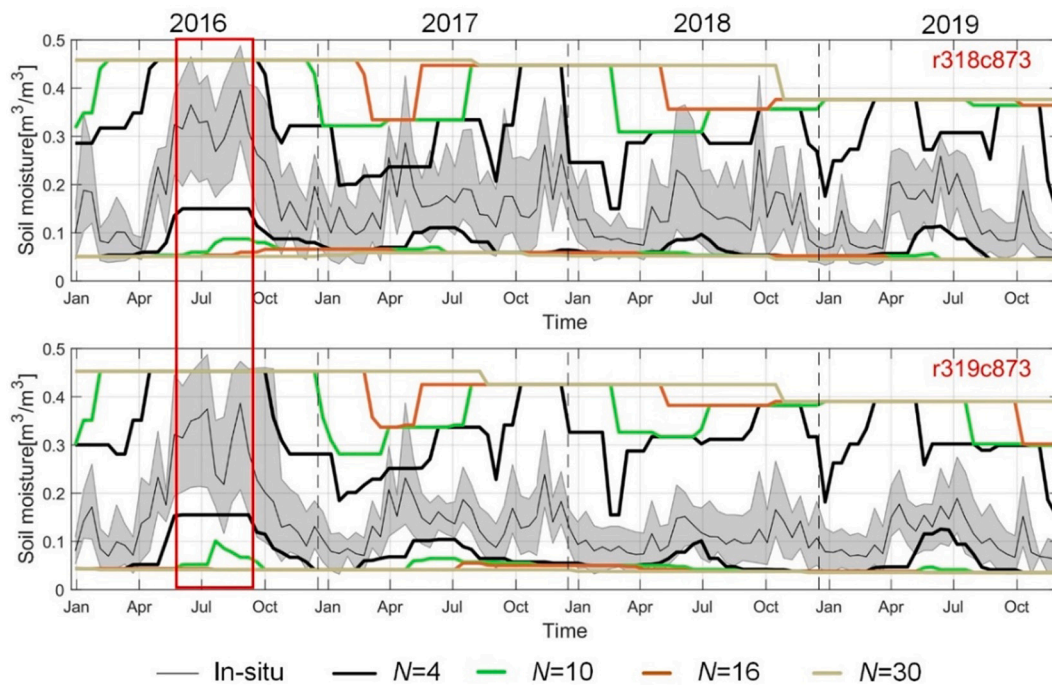
Fig. 7. Examples of soil moisture bounds derived from the SMAP products using an *N* of 4, 10, 16 and 30. The upper and lower boundaries of in-situ station measurements refer to the 10th and 90th percentiles of the OzNet stations.

extracted first. The coarse soil moisture estimates on the 120 Sentinel-1 acquisition dates was then interpolated from the original SMAP time series using a spline function. In the soil moisture retrieval, each interpolated SMAP time series was used to constrain the high resolution retrievals within the 36-km SMAP grid cell.

The Terra and Aqua Moderate Resolution Imaging Spectroradiometer (MODIS) NDVI (MOD13Q1 and MYD13Q1) Version 6 were used to represent the variation of vegetation. The two NDVI sets were produced from optical data collected by two identical sensors, with a spatial resolution of 250 m. Each product used the best available pixel value from all the acquisitions over the 16-day period, eliminating the effect of clouds. In this study, the NDVI data were first combined to have a revisit of 8 days. The composite NDVI were then resampled to 100 m using the nearest neighbor method and re-projected to the EASE-2 36-km grid. The NDVI of each pixel on each Sentinel-1 acquisition date was then calculated using pixel-wise temporal interpolation with a spline function.

3.3. Remote sensing data over the ISMN stations

The GEE was used to prepare the remote sensing data over the 559 stations available from the ISMN, because of its convenience to extract time series data over a large number of stations without downloading and processing the entire tiles/acquisitions of remote sensing images. All the Sentinel-1 IW VV + VH GRD data over each station was extracted from the GEE Sentinel-1 GRD product, which was preprocessed in a similar way to the standard GRD pre-processing workflow (Filipponi, 2019) without terrain correction and flattening. Since the spacing size of GEE Sentinel-1 GRD is 10 m, a buffer of 50 m was used to create the point geometry of each station, and the 10 m pixels within the point geometry averaged to result in an equivalent area of 100 × 100 m². A comparison of the GEE based preprocessing and the preprocessing used for Yanco area showed a root mean square difference of <0.05 dB on the 34 OzNet stations. For some stations, the Sentinel-1 data was collected from different platforms (1A and 1B), orbit passes (ascending or descending), relative orbits (1–175) and thus various incidence and azimuth angles. The extracted time series was thus split into a few sub-

series according to the relative orbit and pass direction to avoid the effect of periodic features and varying incidence angle. Notably, a sub-series of <30 Sentinel-1 acquisitions was removed in order to use a maximum *N* of 30. A summary of the extracted Sentinel-1 time series over each network is provided in Table 1.

The same NDVI products (MOD13Q1 and MYD13Q1 Version 6) were available on the GEE and thus the time series NDVI of each station was extracted and preprocessed in the same way as that for the Yanco area. Since the SMAP products were not available on the GEE, the coarse soil moisture estimates of the ISMN stations were preprocessed locally, being consistent with that of Yanco.

4. Evaluation setup and scenarios

The proposed methods were evaluated under two main scenarios; i) the Yanco agricultural area and ii) globally using the stations available on the ISMN. At Yanco the retrieval performance of the ACD was evaluated with a default *N* of 4 at point, 1-km, and 3-km scales and compared with the SMAP time series. The widely used bias, correlation coefficient (R), root mean square error (RMSE) and unbiased RMSE (ubRMSE) were selected as the indicators of retrieval performance. Globally the ACD was assessed for the effect of temporal vegetation conditions and the extra temporal constraint in soil moisture, along with the effect of vegetation, incidence angle and Sentinel-1 orbit pass using 559 stations. Specifically, five algorithms using different linear equations and constraints were compared, with the details of each algorithm summarized in Table 2.

The STCD method was initially proposed by Balenzano et al. (2011), and modified to include soil moisture bounds (STCD_B) from SMAP products by Ouellette et al. (2017). This study augmented the STCD_B with time-varying vegetation (STCD_V) to remove the assumption of time-invariant vegetation, and the STCD_B with temporal constraints (STCD_T) to force the retrieved soil moisture to follow the trend of SMAP products. The ACD included both the STCD_V and STCD_T modifications with respect to the STCD_B.
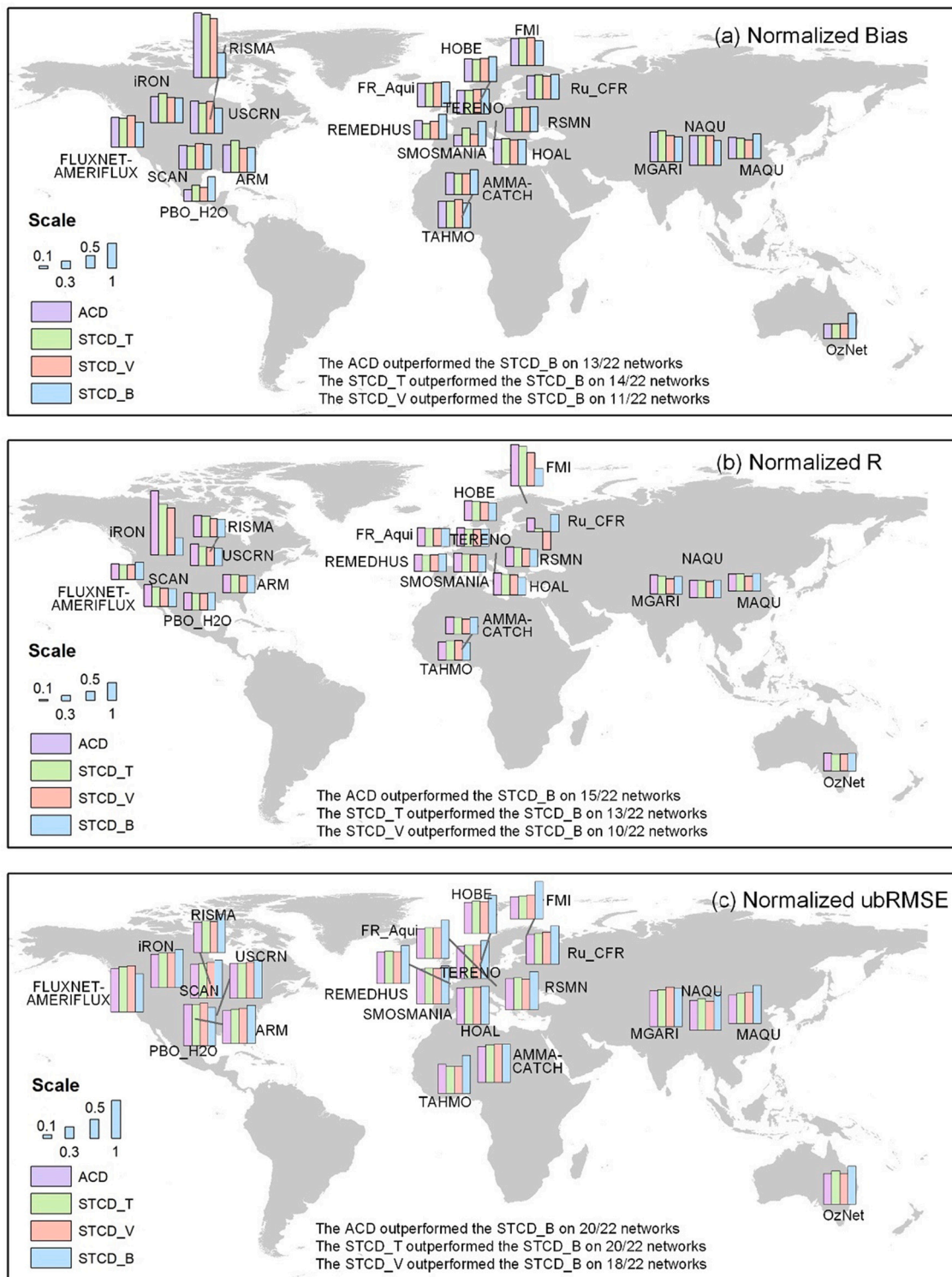
Fig. 8. The normalized performance of ACD, STCD_T, and STCD_V with respect to the STCD_B on the 22 networks using the default $N_t = 4$.

5. Results

5.1. Evaluation using the OzNet data sets

Soil moisture was retrieved using the ACD and compared with the in-situ soil moisture of 34 OzNet stations (Fig. 2a). Acceptable accuracy was achieved with an R and RMSE of 0.664 and 0.072 m^3/m^3, respectively. While the ACD achieved a negligible bias of 0.01 m^3/m^3, substantial overestimation and underestimation was observed at the low

and high end respectively. This may be partly caused by the smaller ranges achieved from the SMAP products. Moreover, the relatively poor performance of high values can be explained by the reduced sensitivity of radar observations to high values. The corresponding Bias, R, RMSE and ubRMSE of the SMAP products were 0.02 m^3/m^3, 0.683, 0.081 m^3/m^3 and 0.079 m^3/m^3 respectively. The improvement in statistics can be mainly from the higher retrieval resolution of ACD. Fig. 2 b depicts the statistics for each station. The RMSE and R of most stations ranged from 0.04 to 0.08 m^3/m^3 and 0.5 to 0.8, with an average value of 0.071 $m^3/$
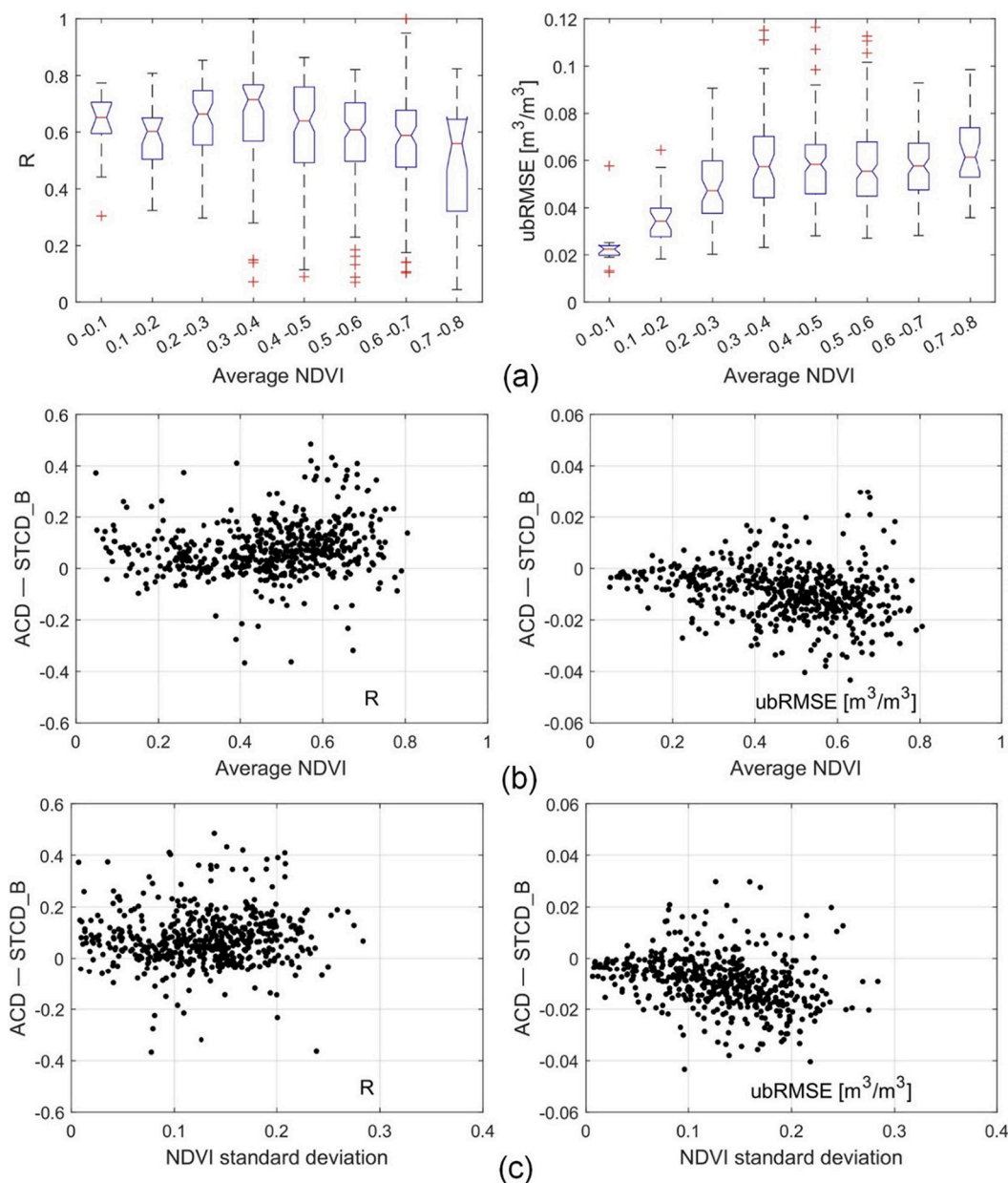
Fig. 9. The performance of ACD with respect to the average of NDVI (a); The performance difference between the ACD and STCD_B versus the average of NDVI (b) and the standard deviation of NDVI (c), with each point representing 1 of the 559 stations. The four-year NDVI of each station was used to calculate the site specific NDVI statistics.

m^3 and 0.68 respectively. The stations in cropping areas showed a higher RMSE and lower R than those in the grazing area. Fifty percent of the cropping stations showed an RMSE of >0.08 m^3/m^3, which is 14% for grazing stations. The soil moisture of grazing stations was generally overestimated, with 19 out of 22 stations having a positive bias. Since the the detailed information of the crop transitions and the crop type from 2016 to 2019 was not available, the effect of vegetation on the retrieval accuracy was investigated using the 559 stations.

Fig. 3 shows the averaged in-situ observations of four 3-km farms (YA4, YA7, YB5, and YB7) and the corresponding averaged soil moisture retrieved by the ACD. In general, the retrieved time series of the four 3-km farms matched well with the in-situ values, resulting in an average R and RMSE of 0.805 and 0.055 m^3/m^3 respectively. However, the ACD underestimated the spatial variation of soil moisture for all four focus farms, with a smaller retrieved standard deviation in most instances. This partly resulted from the mismatch between the real soil moisture

bounds and the bounds achieved from the SMAP products (see the section 5.2). Moreover, stations in cropping areas were all deployed near the edges of individual fields, while the retrieved soil moisture over each site at a resolution of 100 m were often close to the average value of two nearby fields. Therefore, extremely high soil moisture can be recorded by a station after an irrigation event, but a much lower value can be achieved because of the non-irrigated field nearby. This can be another reason for the substantial underestimation observed in YA7 during the period of April 2017 to January 2018.

Fig. 4 shows the averaged in-situ observations of two 36-km EASE-2.0 grids (r318c873 and r319c873) and the corresponding SMAP and retrieved soil moisture. Similar to the comparison over the four 3-km farms, the retrieved soil moisture successfully captured the temporal variation of soil moisture, but failed to fully reflect the inner grid spatial variation. Not surprisingly, the retrieved soil moisture maintained good consistency with the SMAP soil moisture as a result of applying the
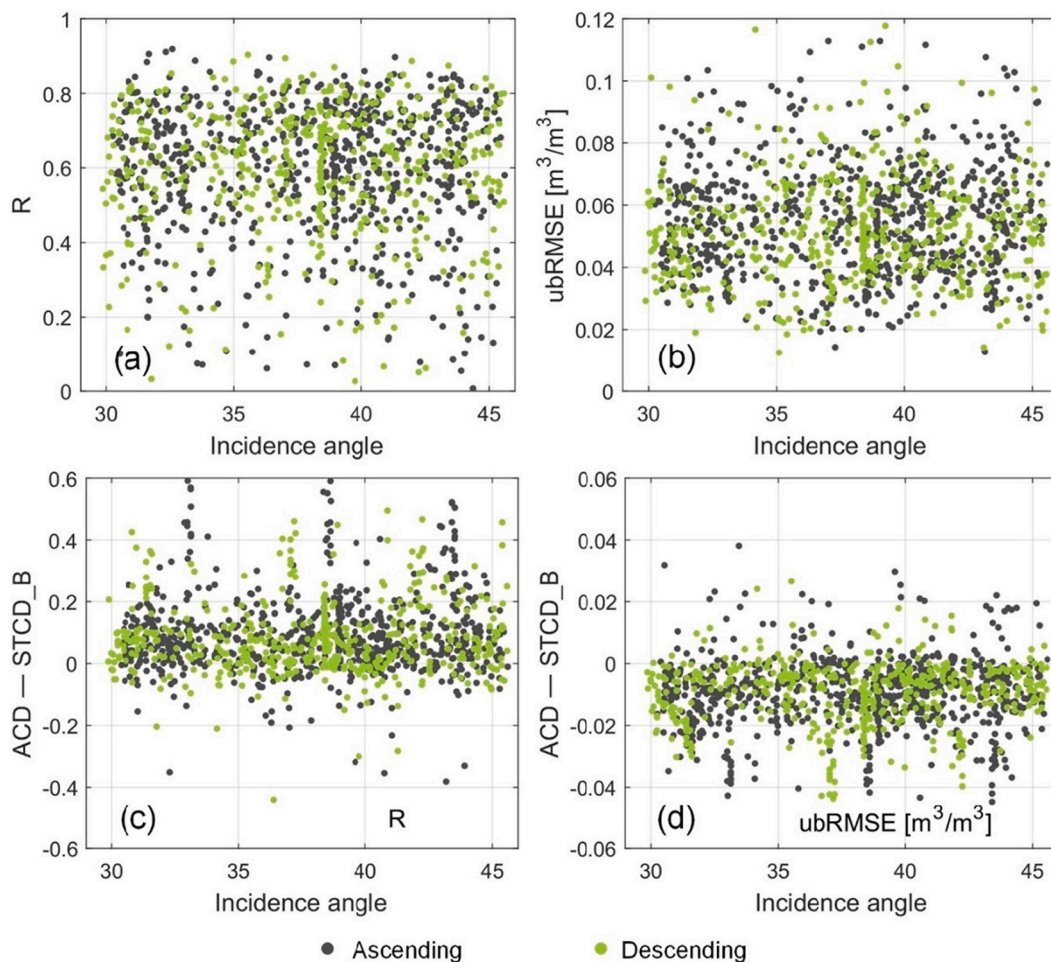
Fig. 10. The effect of incidence angle and orbit direction on the retrieval accuracy of ACD (a, b) and the improvement of using the proposed modifications (c, d). Each point represents a retrieval using a time series with the same incidence angle and orbit direction. A total of 749 ascending and 492 descending time series (Table 1) were used.

SMAP based temporal constraints (Eq. 14). The root mean square difference (RMSD) between the retrieved and SMAP soil moisture was 0.038 m³/m³ and 0.040 m³/m³ for the r318c873 and r319c873 respectively. The largest difference was observed in the rainy season of 2016 when the SMAP soil moisture had much higher values than retrieved and in-situ values. This suggests that the use of mv_{ave} in the calculation of soil moisture bounds (Eq. 12 and 13) can help to maintain a large soil moisture range for a wet season.

5.2. Evaluation using the SMAPEx-5 dataset

Evaluation using the SMAPEx-5 dataset was focused on the spatial distribution of soil moisture at a spatial resolution of 100 m (Fig. 5a) and 1 km (Fig. 5b), with the soil moisture of 1 km being upscaled from that of 0.1 km. Although the evaluation at a fine scale of 0.1 km showed a large RMSE of 0.095 m³/m³, the produced soil moisture maps generally captured the distribution of ground soil moisture measurements. The high soil moisture caused by irrigation events on 27 September were all successfully detected, but at a slightly lower value than the ground measurements. The main reason of such underestimation is likely that the Sentinel-1 acquisition of 27 September (~7 am UTC + 11) was collected at the early stage of the irrigation process whilst the in-situ measurements were collected after irrigation was completed. Moreover, the VWC of these irrigated fields were up to 4 kg/m² during the SMAPEx-5, being another reason of the underestimation.

The soil moisture maps at 1-km resolution generally had consistent

spatial patterns with the ground truth except for a few pixels located in the boundaries of the 3-km farms or that contained irrigated farms. The boundary pixels can only include 1–2 ground samples, while a 1-km mixed pixel of irrigated and non-irrigated areas may not be accurately represented. The scale mismatch between the in-situ and 1-km grid cell was the main reason for the underestimation in comparison (the points in the read circle of Fig. 5b). Accordingly, the real RMSE at 1 km resolution should be much smaller than the reported value of 0.063 m³/m³, being 0.044 m³/m³ after excluding the points in the red circle.

5.3. Effect of retrieval constraints

The performance of the ACD on the 559 ISMN stations was compared with that of the STCD, STCD_B, STCD_T and STCD_V (Table 2) using different N varying from 4 to 30 (Fig. 6 a). The corresponding retrieval time windows ranged from 18 days to 348 days, covering all potential scenarios of time series retrievals. In general, the ACD achieved the best results, followed by the STCD_T, STCD_V, STCD_B and STCD. For the default retrieval scenario of $N = 4$, the R and RMSE of STCD were 0.233 and 0.115 m³/m³ respectively. Accordingly, the soil moisture was substantially underestimated by the STCD with a bias of −0.055 m³/m³, which was compensated by applying SMAP soil moisture bounds (STCD_B). The accuracy was further improved in view of RMSE by considering the time-varying vegetation (STCD_V) and/or using the temporal soil moisture constraint (STCD_T). For other cases of $N > 4$, the RMSE of all five methods increased as N increased, in line with the
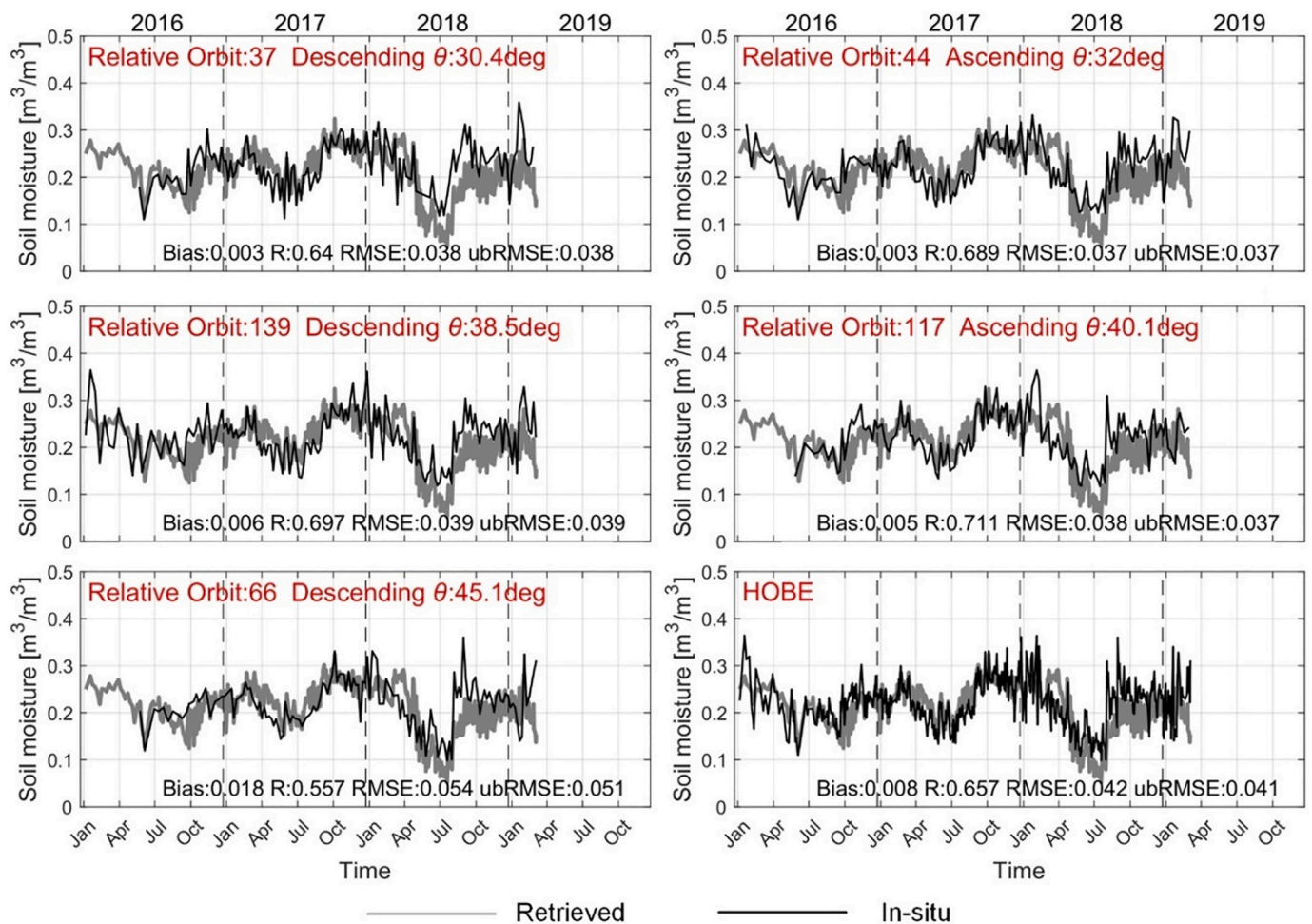
Fig. 11. The retrieved soil moisture time series for the HOBE network, with the six subplots being the results of 5 different orbits and their ensemble average (bottom right). Each time series was the average of the 27 stations of the HOBE network.

results of Palmisano et al. (2020). The methods without the temporal constraint (STCD_V and STCD_B) were more sensitive to N than the ACD and STCD_T. A larger N means more observations and thus reduced uncertainties in solving the linear equations (Eq. 6 or Eq. 9). However, the uncertainty caused by the temporal variation of vegetation and/or soil roughness increased as well. Moreover, the difference between the SMAP soil moisture bounds and the real soil moisture bounds (e.g., the minimum and maximum soil moisture of OzNet stations) increased as N increased (Fig. 7), especially for dry seasons, resulting in poorer retrievals.

Different relationships between R and N were observed for the fives methods, which can be classified into three categories with different soil moisture constraints. The R of the second category (STCD_B and STCD_V) gradually decreased as N increased, consistent with the behavior of RMSE. The R of the first category (STCD) showed a contrary trend, being monotonically increasing from 0.23 to 0.30. As the length of retrieval window increased, the real soil moisture bounds became closer to the default bounds of 0.03 to 0.5 m^3/m^3 (Fig. 7), contributing positively to the R of STCD. This however had a negative effect on the other methods because the soil moisture bounds achieved from the SMAP products had the best estimation of the real soil moisture bounds at $N = 4$, as shown in Fig. 7. Specifically, the STCD becomes the same as STCD_B when the default bounds equal to the SMAP soil moisture bounds in a long enough time window, being the main reason why the R of STCD and STCD_B gradually approached the same value of ~0.30 as N increased.

Different from the first and second category without the temporal

soil moisture constraints, the third category (ACD and STCD_T) achieved a stable R as N increased, in line with the trend of RMSE. The retrieved soil moisture was forced to follow the SMAP time series (Eq. 14) in the ACD and STCD_T, with the error caused by abrupt roughness and/or vegetation changes and the accumulated uncertainty of a long retrieval time window being partly removed. The STCD_V achieved a smaller RMSE than the STCD_B for all cases of N, confirming the effectiveness of the modification to account for time-varying vegetation. However, the ACD only slightly outperformed the STCD_T for a short retrieval window of <10 overpasses.

All five methods achieved large standard deviations for the default retrieval scenario of $N = 4$ (Fig. 6 b), being ~0.08 m^3/m^3 in bias, ~0.2 in R and ~ 0.05 m^3/m^3 in RMSE. As N increased to 30, a limited difference in standard deviation was observed and only the R of STCD showed a large increase, being ~0.08. This may suggest that all five methods had poor stabilities across the 559 stations, being insensitive to the length of retrieval window.

The performance of the ACD, STCD_T, STCD_V, and STCD_B was further analyzed on each network using a default N of 4, with the STCD_B being selected as the benchmark. In the comparison of ACD and STCD_B (Fig. 8), the ACD outperformed the STCD_B on 20 out of the 22 networks in ubRMSE, with the difference being <0.02 m^3/m^3 on most stations. The ACD showed smaller improvements in R, winning on 15 networks. These 15 networks all had relatively smaller R (< 0.65), suggesting that stations with poorer performance can benefit more from using the proposed modifications than those which already had satisfactory performance in STCD_B. The ACD and STCD_B showed similar

biases on all networks, with the bias difference being <0.01 m³/m³ on 21 networks. Similar patterns were observed in the STCD_T versus STCD_B (the second row of Fig. 8) and STCD_V versus STCD_B (the third row of Fig. 8). The STCD_T and STCD_V outperformed 20 and 18 networks in ubRMSE respectively, and the improvement of using either single modification was <0.02 m³/m³ on most networks. The similar patterns observed in Fig. 7 (a-c) may be explained by the marginal utility of either modification when multiple modifications were used.

5.4. Effect of vegetation, incidence angle and look direction on retrieval accuracy

Fig. 9b shows the benefit of using the proposed modifications (i.e., the difference between ACD and STCD_B) under various vegetation status in view of 4-year averaged NDVI. The difference between ACD and STCD_B over bare to sparse vegetation (NDVI <0.4) was smaller than that over more densely vegetated areas (NDVI >0.4). The average improvement in R and ubRMSE was 0.06 and 0.005 m³/m³ respectively for the stations with an average NDVI <0.4, while it was 0.09 and 0.011 m³/m³ for stations with an average NDVI ≥ 0.4. This confirms that the retrieval over dense vegetation can benefit more from the proposed modifications. Since the ACD is expected to partially address the effect of temporal vegetation variations, the relationship between the improvement and the temporal variation of NDVI was investigated in Fig. 9c. For stations with an NDVI standard deviation of <0.1, the average improvement in R and ubRMSE was 0.06 and 0.005 m³/m³ respectively, while it was 0.08 and 0.01 m³/m³ for the rest of the stations. This further confirmed that areas with larger temporal vegetation variations can benefit more using the ACD.

The effect of incidence angle and orbit direction (ascending and descending) was investigated in Fig. 10. In general, the ACD achieved similar performance on time series data collected from various incidence angles (29° to 46°). The average R and ubRMSE of the 749 ascending time series were 0.588 and 0.055 m³/m³ respectively, which was 0.589 and 0.052 m³/m³ for descending time series. Similarly, the performance difference between ACD and STCD_B was insensitive to the incidence angle and orbit direction, with the difference between ascending and descending being 0.015 in R and ~ 0 m³/m³ in ubRMSE.

The HOBE network located in Denmark (Jensen and Refsgaard, 2018) was selected to provide a comparison of the retrieved time series from various orbits (Fig. 11), considering the larger number of available Sentinel-1 orbits at relatively high latitude. The main landcover of the 27 HOBE stations was crop, evergreen forest and mixed forest, with an average NDVI of 0.6. In general, the time series retrieved from 5 orbits well captured the temporal trend of ground measurements. Limited difference was observed among the time series of the 4 orbits with an incidence angle <41°. The time series of orbit 66 showed relatively poorer accuracy statistics and underestimated the short-term temporal variations. This may be explained by the relatively larger effect of vegetation on a larger incidence angle of 45°. The average of the 5 time series showed acceptable accuracy for the network (bottom right of Fig. 11).

6. Conclusion and discussions

An advanced change detection method (ACD) was presented, partly considering the effect of temporal vegetation variation and including an extra temporal constraint in soil moisture with respect to the existing STCD methods (Balenzano et al., 2021; Ouellette et al., 2017). At the default scenario of $N = 4$, the ACD achieved an acceptable RMSE of 0.071 m³/m³, < 0.063 m³/m³ and 0.055 m³/m³ at the point, 1-km and 3-km scales respectively in the Yanco agriculture area. The ACD performed slightly worse than the multi-temporal methods based on well calibrated scattering models at the same research area (Zhu et al., 2020b; Zhu et al., 2019a), but is more promising for operational applications because of its simplicity. While two extra auxiliary data sets

(SMAP soil moisture and MODIS NDVI) are required in the ACD, both are globally available and can be easily prepared using the GEE, allowing the ACD to retain the capability of global operational applications.

The two proposed extensions can be used independently, with their effectiveness confirmed in a comprehensive evaluation using time series observations from 559 stations world-wide. Consideration of either the temporal (STCD_T) or the of time-varying vegetation (STCD_V) constraint can improve the retrieval accuracy with respect to the existing STCD methods. However, the increment in accuracy from using the two modifications was smaller than that from using either modification alone (Fig. 6). This can be explained by i) the benefits of the two modifications being not independent and so the joint benefit is smaller than the summation of the two single modifications alone; and ii) the joint uncertainty of the two modifications is larger than that of either modification. This has also been observed in many other remote sensing applications. For example, the added value of using more spectral bands gradually decreased and evendegraded image classification, being known as curse of dimensionality (Bazi and Melgani, 2009). Although the ACD showed limited improvement with respect to the STCD_T, it is still valuable to use both modifications because implementation of the ACD is as simple as STCD_T or STCD_V alone.

The accuracy statistics of the ACD and other STCD variants on the 559 stations are not particularly satisfying due to the high RMSE (> 0.085 m³/m³). However, the reported RMSE contains spatial representative error, i.e. the error caused by the mismatch between the point measurements and the retrievals at a 100 m pixel. Such error can be 0.02 m³/m³ for validations at 1 km resolution using a single point measurement (Balenzano et al., 2021). This assertion that results are adversely impacted by spatial representation is supported by the detailed evaluation in the Yanco area, where the evaluation for a 1-km grid cell with multiple stations and ground measurements showed an RMSE of <0.063 m³/m³.

The ACD achieved similar performance on data collected from different orbits and/or orbit directions and maintained relatively stable performance for a retrieval window of up to 30 Sentinel-1 acquisitions, being promising for a consistent soil moisture product from different orbits (see Fig. 11 for an example) without cumbersome angular normalization. This can be partly explained by the fact that the crop and soil periodic features change little in a crop season except for abrupt changes caused by, e.g., typhoons. The effect of row features in a short retrieval period on time series backscatter is similar, which is minor in the proposed method. However, both the vegetation and roughness row structures can change substantially during the transitions of crop seasons (Zhu et al., 2020a). The effect of such changes on SAR observations will be erroneously ascribed to the variations of soil moisture, resulting in large errors in retrieval (Zhu et al., 2019c). Moreover, the crop row orientation varies spatially and thus has different scattering mechanisms compared to the same orientation scenario. The effectiveness of the model assumptions also varies spatially, resulting in different retrieval performances.

Despite the advantages of the proposed ACD, Eq. 8 only accounted for the varying vegetation attenuation in time, being still questionable for densely vegetated areas. The sensitivity of Sentinel-1 data to soil moisture and the effectiveness of the existing STCD methods over densely vegetated areas have been comprehensively evaluated (Balenzano et al., 2011; Palmisano et al., 2020). For the area dominated by low density vegetation (e.g., native grass), the attenuated surface scattering dominated the total scattering at C-band VV polarization (Stiles et al., 2000; Zhu et al., 2019a). However, the attenuation caused by low density vegetation was generally small and thus the consideration of time-varying attenuation in Eq. 8 had limited contribution to soil moisture retrieval (Fig. 9). For the densely vegetated area, the received scattering was dominated by the attenuated soil scattering at C-band VV polarization at the early growth stages (Toure et al., 1994), resulting in a similar retrieval scenario of low density vegetation. Moreover, the

double-bounce and volume scattering can be increasingly important as the plant grows, being equivalent to the soil attenuated scattering at the mature stage for an incidence angle >40° (Brown et al., 2003; Palmisano et al., 2020). While an increase in double bounce scattering may maintain the sensitivity of soil moisture (Palmisano et al., 2020), an important effect of increasing volume scattering on soil moisture retrieval is its similarity to that of vegetation attenuation, i.e., reducing the sensitivity of soil moisture to the received backscatter. Accordingly, the use of time-varying attenuation (Eq. 8) can partly compensate the negative effect of time-varying volume and double bounce scattering on change detection methods. However, increasing volume and double bounce scattering can also reduce the correlation between soil moisture and backscatter, which is still unresolved.

Consistent with the existing STCDs, the ACD is not expected to work well for densely vegetated areas. The empirical threshold of −14 dB was therefore used to remove periods dominated by volume scattering, which was based on a few field experiments under various vegetation conditions with incidence angle ranging between 19 and 35° (Satalino et al., 2014). However, the incidence angles in this study ranged from 29 to 41° for the 559 stations, being larger than the data source of the threshold.A more reliable modeling or identification of the volume-dominated area is still challenging due to its multiple dependence on soil surface (row features, moisture), vegetation (types, structure, row orientation, density, phenology), and radar observation geometry. Further studies based on reliable scattering models and ground measurements are thus required to identify the validity range of the proposed method. Alternatively, the empirical relationships between the NDVI and retrieval accuracy (Fig. 9 a) across the 559 stations can be used to suggest the validity of the ACD. Although the effect of time-varying vegetation was not fully considered, Eq. 8 may be the "optimal" extension to the existing STCD methods considering the tradeoff between the complexity of modeling the time-varying vegetation scattering and the feasibility of operational soil moisture retrieval. Since ground vegetation samples of a complete crop season were not available for the Yanco area, the contribution of ACD under different vegetation conditions were investigated using 559 worldwide stations, confirming that the retrievals over densely vegetated area or areas with large temporal vegetation variation can benefit more from the ACD.

It's worth highlighting the disadvantages of the SMAP soil moisture bounds and the temporal constraint (Eq. 14) though it substantially improved the retrieval accuracy (Fig. 6). The SMAP soil moisture over the retrieval period was found to provide a reliable estimation of the soil moisture bounds observed by the OzNet stations (Fig. 7). However, the global minimum soil moisture of SMAP was larger than that of OzNet, resulting in a substantial overestimation in low values. Moreover, the relatively smaller range of SMAP soil moisture at the suggested scenario ($N = 4$) resulted in a smaller retrieved soil moisture range (Fig. 2 a and Fig. 5 a) and a smaller spatial variation (Fig. 3 and Fig. 4). This was

especially true for irrigated farms in dry seasons (e.g., the period of April to July 2017), where the range of SMAP soil moisture was much smaller than that of real soil moisture (Fig. 7). The use of historical averaged SMAP (the mv_{ave} in Eq. 12 and 13) was found to partly compensate the mismatch between the range of SMAP soil moisture in time and the range of real soil moisture spatially, being still insufficient for the aforementioned special cases.

The empirical threshold of VV > −1 dB was used to detect highly confident irrigation and sub-grid rainfall events, based on empirical studies over part of Europe (Bazzi et al., 2020). However, a small rainfall event may slightly change the soil moisture, with the increase in backscatter <1 dB. Similarly, the empirical threshold of NDVI >0.2 can introduce uncertainty in identifying vegetated areas, but can have limited effect on the retrievals considering the limited attenuation at the soil-vegetation transition regime. Fig. 9 shows limited performance difference between ACD and STCD_B near the NDVI threshold of 0.2. Sophisticated methods for detecting the irrigation, rainfall, vegetation and areas dominated by volume scattering are a favorable alternative (Zhu et al., 2019c) but can be too complex for integration in the ACD. Consequently, the main reason for using these literature-based empirical thresholds is in maintaining the ability of operational application, which is as important as improvement in accuracy, with this capability being demonstrated on 559 world-wide stations.

CRediT authorship contribution statement

Liujun Zhu: Conceptualization, Methodology, Writing – original draft. **Rui Si:** Writing – original draft, Writing – review & editing. **Xiaoji Shen:** Writing – review & editing. **Jeffrey P. Walker:** Writing – review & editing.

Declaration of Competing Interest

Liujun Zhu reports financial support was provided by Hohai Unversity.

Acknowledgments

Appendix A. Appendix

Given a time series of N Sentinel-1 VV acquisitions, $N − 1$ temporal ratios of $S_{2,1}, \dots S_{i+1,i}, \dots S_{N,N-1}$ can be calculated using Eq. 8:

$$S_{i+1,i} \approx \frac{|\alpha_{i+1}|^2 exp(-2AV_{i+1}sec\theta)}{|\alpha_i|^2 exp(-2AV_i sec\theta)} \tag{A1}$$

After applying the log transform on both sides, $S_{i+1,i}$ was written in a linear form:

$$ln(S_{i+1,i}) - 2ln(\alpha_{i+1}) + 2ln(\alpha_i) = -2A(V_{i+1} - V_i)sec\theta \tag{A2}$$

Together with the linear form of $S_{i+2,i+1}$, the incidence angle θ and empirical parameter A were eliminated:

$$\frac{ln(S_{i+1,i}) - 2ln(\alpha_{i+1}) + 2ln(\alpha_i)}{ln(S_{i+2,i+1}) - 2ln(\alpha_{i+2}) + 2ln(\alpha_{i+1})} = \frac{V_{i+1} - V_i}{V_{i+2} - V_{i+1}}, V_{i+2} \neq V_{i+1} \tag{A3}$$

or

$$\frac{ln\left(S_{i+2,i+1}\right) - 2ln(\alpha_{i+2}) + 2ln(\alpha_{i+1})}{ln\left(S_{i+1,i}\right) - 2ln(\alpha_{i+1}) + 2ln(\alpha_i)} = \frac{V_{i+2} - V_{i+1}}{V_{i+1} - V_i}, V_{i+1} \neq V_i \tag{A4}$$

The matrix form of Eq. A3 and Eq. A4 thus are:

$$\left[-2 \quad 2\omega_{i+2,i} + 2 \quad -2\omega_{i+2,i}\right]\left[ln(\alpha_i) \quad ln(\alpha_{i+1}) \quad ln(\alpha_{i+2})\right]^{\mathrm{T}} = ln\left(S_{i+1,i}\right) - \omega_{i+2,i}ln\left(S_{i+2,i+1}\right) \tag{A5}$$

with

$$\omega_{i+2,i} = (V_{i+1} - V_i)/(V_{i+2} - V_{i+1}), (V_{i+2} \neq V_{i+1}) \tag{A6}$$

or

$$\left[2\omega_{i+2,i} - 2 \quad 2 \quad -2\omega_{i+2,i}\right]\left[ln(\alpha_i) \quad ln(\alpha_{i+1}) \quad ln(\alpha_{i+2})\right]^{\mathrm{T}} = ln\left(S_{i+1,i}\right) - \omega_{i+2,i}ln\left(S_{i+2,i}\right) \tag{A7}$$

with

$$\omega_{i+2,i} = (V_{i+1} - V_i)/(V_{i+2} - V_i), (V_{i+2} = V_{i+1}) \tag{A8}$$

For a special period of bare soil or soil covered by time-invariant vegetation (i.e., $Vi + 2 = Vi + 1 = Vi$), two equations can be obtained:

$$\left[-2 \quad 2 \quad 0\right]\left[ln(\alpha_i) \quad ln(\alpha_{i+1}) \quad ln(\alpha_{i+2})\right]^{\mathrm{T}} = ln\left(S_{i+1,i}\right) \tag{A9}$$

and

$$\left[0 \quad -2 \quad 2\right]\left[ln(\alpha_i) \quad ln(\alpha_{i+1}) \quad ln(\alpha_{i+2})\right]^{\mathrm{T}} = ln\left(S_{i,i-1}\right) \tag{A10}$$

The Eq. A5 – A10 can then be used to build a linear underdetermined system of $N - 2$ or $N - 1$ equations with N unknowns $ln(\alpha_N)$ according to the time series vegetation descriptors ($V_1, \ldots V_i, \ldots V_N$). In this study, the function "lsqlin" with the default setups provided in the MATLAB was used, which is a subspace trust-region method based on the interior-reflective Newton method.

References

Acevedo, E., Silva, P., Silva, H., 2002. Wheat growth and physiology. Bread Wheat Improv. Product. 30, 39–70.

Al-Khaldi, M.M., Johnson, J.T., O'Brien, A.J., Balenzano, A., Mattia, F., 2019. Time-series retrieval of soil moisture using CYGNSS. IEEE Trans. Geosci. Remote Sens. 57, 4322–4331.

Al-Yaari, A., Dayau, S., Chipeaux, C., Aluome, C., Kruszewski, A., Loustau, D., Wigneron, J.-P., 2018. The AQUI soil moisture network for satellite microwave remote sensing validation in South-Western France. Remote Sens. 10, 1839.

Attema, E., Ulaby, F.T., 1978. Vegetation modeled as a water cloud. Radio Sci. 13, 357–364.

Balenzano, A., Mattia, F., Satalino, G., Davidson, M.W., 2011. Dense temporal series of C- and L-band SAR data for soil moisture retrieval over agricultural crops. IEEE J. Select. Top. Appl. Earth Observ. Remote Sens. 4, 439–450.

Balenzano, A., Mattia, F., Satalino, G., Pauwels, V., Snoeij, P., 2012. SMOSAR algorithm for soil moisture retrieval using Sentinel-1 data. In: IEEE Geoscience and Remote Sensing Symposium (IGARSS). IEEE, pp. 1200–1203. 2012.

Balenzano, A., Satalino, G., Lovergine, F., Rinaldi, M., Iacobellis, V., Mastronardi, N., Mattia, F., 2013. On the use of temporal series of L-and X-band SAR data for soil moisture retrieval. Capitanata plain case study. Eur. J. Remote Sens. 46, 721–737.

Balenzano, A., Mattia, F., Satalino, G., Lovergine, F.P., Palmisano, D., Peng, J., Marzahn, P., Wegmüller, U., Cartus, O., Dąbrowska-Zielińska, K., 2021. Sentinel-1 soil moisture at 1 km resolution: a validation study. Remote Sens. Environ. 263, 112554.

Bartalis, Z., Wagner, W., Naeimi, V., Hasenauer, S., Scipal, K., Bonekamp, H., Figa, J., Anderson, C., 2007. Initial soil moisture retrievals from the METOP-A advanced scatterometer (ASCAT). Geophys. Res. Lett. 34.

Bauer-Marschallinger, B., Freeman, V., Cao, S., Paulik, C., Schaufler, S., Stachl, T., Modanesi, S., Massari, C., Ciabatta, L., Brocca, L., 2018. Toward global soil moisture monitoring with Sentinel-1: harnessing assets and overcoming obstacles. IEEE Trans. Geosci. Remote Sens. 57, 520–539.

Bazi, Y., Melgani, F., 2009. Gaussian process approach to remote sensing image classification. IEEE Trans. Geosci. Remote Sens. 48, 186–197.

Bazzi, H., Baghdadi, N., Fayad, I., Zribi, M., Belhouchette, H., Demarez, V., 2020. Near real-time irrigation detection at plot scale using sentinel-1 data. Remote Sens. 12, 1456.

Bell, J.E., Palecki, M.A., Baker, C.B., Collins, W.G., Lawrimore, J.H., Leeper, R.D., Hall, M.E., Kochendorfer, J., Meyers, T.P., Wilson, T., 2013. US Climate Reference Network soil moisture and temperature observations. J. Hydrometeorol. 14, 977–988.

Blöschl, G., Blaschke, A., Broer, M., Bucher, C., Carr, G., Chen, X., Eder, A., Exner-Kittridge, M., Farnleitner, A., Flores-Orozco, A., 2016. The hydrological open air laboratory (HOAL) in Petzenkirchen: a hypothesis-driven observatory. Hydrol. Earth Syst. Sci. 20, 227–255.

Bousbih, S., Zribi, M., El Hajj, M., Baghdadi, N., Lili-Chabaane, Z., Gao, Q., Fanise, P., 2018. Soil moisture and irrigation mapping in a semi-arid region, based on the synergetic use of Sentinel-1 and Sentinel-2 data. Remote Sens. 10, 1953.

Brown, S.C., Quegan, S., Morrison, K., Bennett, J.C., Cookmartin, G., 2003. High-resolution measurements of scattering in wheat canopies-implications for crop parameter retrieval. IEEE Trans. Geosci. Remote Sens. 41, 1602–1610.

Buchhorn, M., Lesiv, M., Tsendbazar, N.-E., Herold, M., Bertels, L., Smets, B., 2020. Copernicus global land cover layers—collection 2. Remote Sens. 12, 1044.

Callens, M., Verhoest, N.E., Davidson, M.W., 2006. Parameterization of tillage-induced single-scale soil roughness from 4-m profiles. IEEE Trans. Geosci. Remote Sens. 44, 878–888.

Calvet, J.-C., Fritz, N., Berne, C., Piguet, B., Maurel, W., Meurey, C., 2016. Deriving pedotransfer functions for soil quartz fraction in southern France from reverse modeling. Soil 2, 615–629.

Cook, D.R., 2016. Soil temperature and moisture profile (STAMP) system handbook. In: DOE Office of Science Atmospheric Radiation Measurement (ARM) Program.

Cui, H., Jiang, L., Paloscia, S., Santi, E., Pettinato, S., Wang, J., Fang, X., Liao, W., 2021. The potential of ALOS-2 and Sentinel-1 radar data for soil moisture retrieval with high spatial resolution over agroforestry areas, China. IEEE Trans. Geosci. Remote Sens. 60, 1–17.

Dobson, M.C., Ulaby, F.T., Hallikainen, M.T., El-Rayes, M., 1985. Microwave dielectric behavior of wet soil-part II: dielectric mixing models. IEEE Trans. Geosci. Remote Sens. 35–46.

Dorigo, W., Wagner, W., Albergel, C., Albrecht, F., Balsamo, G., Brocca, L., Chung, D., Ertl, M., Forkel, M., Gruber, A., 2017. ESA CCI soil moisture for improved earth system understanding: state-of-the art and future directions. Remote Sens. Environ. 203, 185–215.

Dorigo, W., Himmelbauer, I., Aberer, D., Schremmer, L., Petrakovic, I., Zappa, L., Preimesberger, W., Xaver, A., Annor, F., Ardö, J., 2021. The international soil moisture network: serving earth system science for over a decade. Hydrol. Earth Syst. Sci. 25, 5749–5804.

El Hajj, M., Baghdadi, N., Zribi, M., Belaud, G., Cheviron, B., Courault, D., Charron, F., 2016. Soil moisture retrieval over irrigated grassland using X-band SAR data. Remote Sens. Environ. 176, 202–218.

Entekhabi, D., Njoku, E.G., O'Neill, P.E., Kellogg, K.H., Crow, W.T., Edelstein, W.N., Entin, J.K., Goodman, S.D., Jackson, T.J., Johnson, J., 2010. The soil moisture active passive (SMAP) mission. Proc. IEEE 98, 704–716.

Fan, D., Zhao, T., Jiang, X., Xue, H., Moukomla, S., Kuntiyawichai, K., Shi, J., 2021. Soil moisture retrieval from Sentinel-1 time-series data over croplands of Northeastern Thailand. In: Ieee Geoscience and Remote Sensing Letters.

Filipponi, F., 2019. Sentinel-1 GRD preprocessing workflow. In: Multidisciplinary Digital Publishing Institute Proceedings, p. 11.

Galle, S., Grippa, M., Peugeot, C., Moussa, I.B., Cappelaere, B., Demarty, J., Mougin, E., Panthou, G., Adjomayi, P., Agbossou, E., 2018. AMMA-CATCH, a critical zone observatory in West Africa monitoring a region in transition. Vadose Zone J. 17, 1–24.

Gao, Q., Zribi, M., Escorihuela, M.J., Baghdadi, N., 2017. Synergetic use of Sentinel-1 and Sentinel-2 data for soil moisture mapping at 100 m resolution. Sensors 17, 1966.

González-Zamora, Á., Sánchez, N., Pablos, M., Martínez-Fernández, J., 2019. CCI soil moisture assessment with SMOS soil moisture and in situ data under different environmental conditions and spatial scales in Spain. Remote Sens. Environ. 225, 469–482.

He, L., Qin, Q., Panciera, R., Tanase, M., Walker, J.P., Hong, Y., 2017. An extension of the alpha approximation method for soil moisture estimation using time-series SAR data over bare soil surfaces. IEEE Geosci. Remote Sens. Lett. 14, 1328–1332.

Ikonen, J., Smolander, T., Rautiainen, K., Cohen, J., Lemmetyinen, J., Salminen, M., Pulliainen, J., 2018. Spatially distributed evaluation of ESA CCI Soil Moisture products in a northern boreal forest environment. Geosciences 8, 51.

Jackson, T., McNairn, H., Weltz, M., Brisco, B., Brown, R., 1997. First order surface roughness correction of active microwave observations for estimating soil moisture. IEEE Trans. Geosci. Remote Sens. 35, 1065–1069.

Jensen, K.H., Refsgaard, J.C., 2018. HOBE: the Danish hydrological observatory. Vadose Zone J. 17, 1–24.

Joseph, A., van der Velde, R., O'Neill, P., Lang, R., Gish, T., 2010. Effects of corn on C- and L-band radar backscatter: a correction method for soil moisture retrieval. Remote Sens. Environ. 114, 2417–2430.

Kerr, Y.H., Waldteufel, P., Wigneron, J.-P., Delwart, S., Cabot, F., Boutin, J., Escorihuela, M.-J., Font, J., Reul, N., Gruhier, C., 2010. The SMOS mission: new tool for monitoring key elements ofthe global water cycle. Proc. IEEE 98, 666–687.

Kim, S.-B., Tsang, L., Johnson, J.T., Huang, S., Van Zyl, J., Njoku, E.G., 2012. Soil moisture retrieval using time-series radar observations over bare surfaces. IEEE Trans. Geosci. Remote Sens. 50, 1853–1863.

Kornelsen, K.C., Coulibaly, P., 2013. Advances in soil moisture retrieval from synthetic aperture radar and hydrological applications. J. Hydrol. 476, 460–489.

Larson, K.M., Small, E.E., Gutmann, E.D., Bilich, A.L., Braun, J.J., Zavorotny, V.U., 2008. Use of GPS receivers as a soil moisture network for water cycle studies. Geophys. Res. Lett. 35.

Merlin, O., Walker, J., Panciera, R., Young, R., Kalma, J., Kim, E., 2007. Calibration of a soil moisture sensor in heterogeneous terrain. In: Oxley, L., Kulasiri, D. (Eds.), 2007 International Congress on Modelling and Simulation (MODSIM). Modelling and Simulation Society of Australia and New Zealand, pp. 2604–2610.

Montandon, L., Small, E., 2008. The impact of soil reflectance on the quantification of the green vegetation fraction from NDVI. Remote Sens. Environ. 112, 1835–1845.

Neill, O., Chan, S., Njoku, E.G., Jackson, T., Bindlish, R., Chaubell, J., 2019. SMAP L3 radiometer global daily 36 km EASE-grid soil moisture. In: N.N.S.a.I.D.C.D.A.A. Center (Ed.).

Njoku, E.G., Wilson, W.J., Yueh, S.H., Dinardo, S.J., Li, F.K., Jackson, T.J., Lakshmi, V., Bolten, J., 2002. Observations of soil moisture using a passive and active low-frequency microwave airborne sensor during SGP99. IEEE Trans. Geosci. Remote Sens. 40, 2659–2673.

Ojo, E.R., Bullock, P.R., L'Heureux, J., Powers, J., McNairn, H., Pacheco, A., 2015. Calibration and evaluation of a frequency domain reflectometry sensor for real-time soil moisture monitoring. Vadose Zone J. 14.

Osenga, E., Arnott, J.C., Endsley, K.A., Katzenberger, J., 2019. Bioclimatic and soil moisture monitoring across elevation in a mountain watershed: opportunities for research and resource management. Water Resour. Res. 55, 2493–2503.

Ouellette, J.D., Johnson, J.T., Balenzano, A., Mattia, F., Satalino, G., Kim, S.-B., Dunbar, R.S., Colliander, A., Cosh, M.H., Caldwell, T.G., 2017. A time-series approach to estimating soil moisture from vegetated surfaces using L-band radar backscatter. IEEE Trans. Geosci. Remote Sens. 55, 3186–3193.

Palmisano, D., Mattia, F., Balenzano, A., Satalino, G., Pierdicca, N., Guarnieri, A.V.M., 2020. Sentinel-1 sensitivity to soil moisture at high incidence angle and the impact on retrieval over seasonal crops. In: Ieee Transactions on Geoscience and Remote Sensing.

Paloscia, S., Pettinato, S., Santi, E., Notarnicola, C., Pasolli, L., Reppucci, A., 2013. Soil moisture mapping using Sentinel-1 images: algorithm and preliminary validation. Remote Sens. Environ. 134, 234–248.

Peng, J., Loew, A., Merlin, O., Verhoest, N.E., 2017. A review of spatial downscaling of satellite remotely sensed soil moisture. Rev. Geophys. 55, 341–366.

Peng, J., Albergel, C., Balenzano, A., Brocca, L., Cartus, O., Cosh, M.H., Crow, W.T., Dabrowska-Zielinska, K., Dadson, S., Davidson, M.W., 2020. A roadmap for high-resolution satellite soil moisture applications–confronting product characteristics with user requirements. Remote Sens. Environ. 112162.

Pierdicca, N., Pulvirenti, L., Bignami, C., 2010. Soil moisture estimation over vegetated terrains using multitemporal remote sensing data. Remote Sens. Environ. 114, 440–448.

Qiu, J., Crow, W.T., Wagner, W., Zhao, T., 2019. Effect of vegetation index choice on soil moisture retrievals via the synergistic use of synthetic aperture radar and optical remote sensing. Int. J. Appl. Earth Obs. Geoinf. 80, 47–57.

Sabaghy, S., Walker, J.P., Renzullo, L.J., Jackson, T.J., 2018. Spatially enhanced passive microwave derived soil moisture: capabilities and opportunities. Remote Sens. Environ. 209, 551–580.

Satalino, G., Balenzano, A., Mattia, F., Davidson, M.W., 2014. C-band SAR data for mapping crops dominated by surface or volume scattering. IEEE Geosci. Remote Sens. Lett. 11, 384–388.

Schaefer, G.L., Cosh, M.H., Jackson, T.J., 2007. The USDA natural resources conservation service soil climate analysis network (SCAN). J. Atmos. Ocean. Technol. 24, 2073–2077.

Smith, A., Walker, J., Western, A., Young, R., Ellett, K., Pipunic, R., Grayson, R., Siriwardena, L., Chiew, F., Richter, H., 2012. The Murrumbidgee soil moisture monitoring network data set. Water Resour. Res. 48.

Stiles, J.M., Sarabandi, K., Ulaby, F.T., 2000. Electromagnetic scattering from grassland. II. Measurement and modeling results. IEEE Trans. Geosci. Remote Sens. 38, 349–356.

Su, Z., Wen, J., Dente, L., Van Der Velde, R., Wang, L., Ma, Y., Yang, K., Hu, Z., 2011. The Tibetan Plateau observatory of plateau scale soil moisture and soil temperature (Tibet-Obs) for quantifying uncertainties in coarse resolution satellite and model products. Hydrol. Earth Syst. Sci. 15, 2303–2316.

Tomer, S.K., Al Bitar, A., Sekhar, M., Zribi, M., Bandyopadhyay, S., Sreelash, K., Sharma, A., Corgne, S., Kerr, Y., 2015. Retrieval and multi-scale validation of soil moisture from multi-temporal SAR data in a semi-arid tropical region. Remote Sens. 7, 8128–8153.

Torres, R., Snoeij, P., Geudtner, D., Bibby, D., Davidson, M., Attema, E., Potin, P., Rommen, B., Floury, N., Brown, M., 2012. GMES Sentinel-1 mission. Remote Sens. Environ. 120, 9–24.

Toure, A., Thomson, K.P., Edwards, G., Brown, R.J., Brisco, B.G., 1994. Adaptation of the MIMICS backscattering model to the agricultural context-wheat and canola at L and C bands. IEEE Trans. Geosci. Remote Sens. 32, 47–61.

Wagner, W., Lemoine, G., Borgeaud, M., Rott, H., 1999a. A study of vegetation cover effects on ERS scatterometer data. IEEE Trans. Geosci. Remote Sens. 37, 938–948.

Wagner, W., Lemoine, G., Rott, H., 1999b. A method for estimating soil moisture from ERS scatterometer and soil data. Remote Sens. Environ. 70, 191–207.

Yao, P., Lu, H., Shi, J., Zhao, T., Yang, K., Cosh, M.H., Gianotti, D.J.S., Entekhabi, D., 2021. A long term global daily soil moisture dataset derived from AMSR-E and AMSR2 (2002–2019). Scientific data 8, 1–16.

Ye, N., Walker, J.P., Wu, X., Jeu, R.D., Gao, Y., Jackson, T.J., Jonard, F., Kim, E., Merlin, O., Pauwels, V., Renzullo, L.J., Rüdiger, C., Sabaghy, S.C., Hebel, V., Yueh, S.H., Zhu, L., 2020. The soil moisture active passive experiments: validation of the SMAP products in Australia. IEEE Trans. Geosci. Remote Sens. 59, 2922–2939.

Zacharias, S., Bogena, H., Samaniego, L., Mauder, M., Fuß, R., Pütz, T., Frenzel, M., Schwank, M., Baessler, C., Butterbach-Bahl, K., 2011. A network of terrestrial environmental observatories in Germany. Vadose Zone J. 10, 955–973.

Zhu, L., Walker, J.P., Tsang, L., Huang, H., Ye, N., Rüdiger, C., 2019a. A multi-frequency framework for soil moisture retrieval from time series radar data. Remote Sens. Environ. 235, 111433.

Zhu, L., Walker, J.P., Tsang, L., Huang, H., Ye, N., Rüdiger, C., 2019b. Soil moisture retrieval from time series multi-angular radar data using a dry down constraint. Remote Sens. Environ. 231, 111237.

Zhu, L., Walker, J.P., Ye, N., Rüdiger, C., 2019c. Roughness and vegetation change detection: a pre-processing for soil moisture retrieval from multi-temporal SAR imagery. Remote Sens. Environ. 225, 93–106.

Zhu, L., Walker, J.P., Rdiger, C., Xiao, P., 2020a. Identification of agricultural row features using optical data for scattering and reflectance modelling over periodic surfaces. Ieee J. Select. Top. Appl. Earth Observ. Remote Sens. 13, 1729–1739.

Zhu, L., Walker, J.P., Shen, X., 2020b. Stochastic ensemble methods for multi-SAR-mission soil moisture retrieval. Remote Sens. Environ. 251, 112099.

Zribi, M., Foucras, M., Baghdadi, N., Demarty, J., Muddu, S., 2020. A new reflectivity index for the retrieval of surface soil moisture from radar data. Ieee J. Select. Top. Appl. Earth Observ. Remote Sens. 14, 818–826.